CLM-P625

UKAEA

Preprint

A STUDY OF THE EFFECT OF IMPURITY RADIATION FROM THE PERIPHERAL PLASMA OF A TOKAMAK REACTOR

D. E. T. F. ASHBY
M. H. HUGHES

CULHAM LABORATORY
Abingdon Oxfordshire

1980

ERRATA

CLM-P625

A STUDY OF THE EFFECT OF IMPURITY IRRADIATION FROM THE PERIPHERAL PLASMA OF A TOKAMAK REACTOR

D.E.T.F. Ashby
M.H. Hughes

Page 22 Eqn.35 should read

$$I^2 \eta \, 2R/a^2 = 2\pi R \pi a^2 \; 3n\overline{T}/\tau_E$$

Eqns. 37 and 38 should read

$$q^{-1} < 4.6 \times 10^{-33} \left\{ \frac{Rn}{B} e \left(B \frac{a}{R} \right)^{2/5} \right\}^{5/3} F\left(Z_{eff}\right) \qquad (37)$$

where $F\left(Z_{eff}\right) = \left(Z_{eff}^{-1}\right)^{5/6} \left[\gamma \left(Z_{eff} \right) \right]^{-1/2}$

$$= \left(Z_{eff}^{-1}\right)^{5/6} \left\{ Z_{eff} \left[.29 + .46/\left(1.08 + Z_{eff}\right) \right] \right\}^{-1/2} \qquad (38)$$

CLM-P625

A STUDY OF THE EFFECT OF IMPURITY RADIATION FROM THE PERIPHERAL PLASMA OF A TOKAMAK REACTOR

by

D.E.T.F.Ashby and M.H.Hughes, Culham Laboratory, Abingdon, Oxon.(Euratom/ UKAEA Fusion Association)United Kingdom.

ABSTRACT

If the power lost by impurity radiation from the low temperature boundary region of a confined plasma exceeds the power transported from the central region then temperature equilibrium is impossible and the temperature profile will collapse. This situation is studied on the assumption of coronal equilibrium and the results are used to predict the permissible impurity concentration at the edge of a Tokamak Reactor. The effect of neoclassical impurity transport is studied analytically and a 1D tokamak diffusion code is used to illustrate the detailed collapse of the temperature profile when the plasma density in a radiation-cooled tokamak is increased. Finally the results are used to predict the limiting density of a radiation-cooled tokamak; this predicted density limit is compared with the density limits observed in current tokamak experiments.

(To be submitted to Nuclear Fusion)

November 1980

1. INTRODUCTION

Several authors have examined the effect of impurity radiation on the performance of conceptual fusion reactors e.g.[1-4]. They have all considered the power radiated from the bulk of the plasma and its effect on energy confinement time and power balance. In contrast this paper deals solely with radiation from the peripheral low temperature plasma in a Tokamak Reactor. This low temperature plasma can be expected to radiate more power than the central plasma since impurity line radiation peaks when $T \lesssim 0.1 - 1\text{keV}$ whereas in the bulk plasma, where $T \approx 10\text{keV}$, all but heavy impurities are fully-stripped and the radiation is mainly bremsstrahlung.

The importance of radiation from the peripheral region arises as follows. The power radiated is supplied by transport from the hot central plasma where, in a reactor, fusion generates alpha particles which are subsequently thermalized. If the radiated power exceeds that transported from

the central region then temperature equilibrium is impossible and the peripheral region must cool causing the temperature profile to collapse. Temperature profile collapse due to radiation cooling of the peripheral plasma is thought to be one cause of the disruptive instability observed in current tokamak experiments [5-8].

In this paper we derive a simple criterion for the onset of temperature profile collapse in tokamaks and consider the thermal stability of a radiation-cooled reactor. We consider analytically the effect of neoclassical impurity transport and then examine temporal behaviour by computer modelling the conceptual test reactor INTOR. Finally, on the assumption that temperature collapse will lead to a disruptive instability, we consider the density limits implied and compare them with the limits observed in current tokamak experiments.

2. PERIPHERAL RADIATION AND TEMPERATURE PROFILE

Consider the narrow peripheral region of a fusion reactor where $T \lesssim 2\text{keV}$. There are no major energy sources in this plasma so, if electron thermal conduction is the dominant transport mechanism, the equilibrium temperature profile is determined by

$$\frac{d}{dr}\left(\kappa_e \frac{dT}{dr}\right) = n_e n_z L(T) \qquad (1)$$

where n_e and n_z are the electron and impurity densities respectively and $L(T)$ describes the radiation loss.

Integrating eqn. (1) gives

$$\left(\kappa_e \frac{dT}{dr}\right)_1^2 - \left(\kappa_e \frac{dT}{dr}\right)_0^2 = 2\int_0^{T_1} \kappa_e\, n_e\, n_z\, L(T)\,dT \qquad (2)$$

If all the power conducted from the central region is radiated by the peripheral plasma then $(\kappa_e dT/dr)_o = 0$ and eqn.(2) becomes

$$Q_1^2 = (\kappa_e dT/dr)_1^2 = 2\int_0^{T_1} \kappa_e\, n_e\, n_z\, L(T)\, dT \qquad (3)$$

If the thermal flux Q_1 is too small to satisfy this equation then no steady solution exists with $\kappa_e dT/dr = 0$ at $T = 0$; hence temperature equilibrium is impossible and the temperature profile collapses. Eqn.3 can be simplified by assuming that κ_e, n_e and n_z are constant thus giving the following condition for the onset of temperature profile collapse

$$Q_1^2 < 2\kappa_e\, n_e\, n_z \int_0^{T_1} L(T)dT \qquad (3a)$$

Note that 'Alcator scaling' of energy confinement time (i.e. $\tau_E \propto na^2$) is consistent with κ_e = constant and that the variation in n_e and n_z is likely to be much less than that in L(T) which typically changes by two orders of magnitude.

Post et al [9] have evaluated L(T) for a number of elements from an 'average ion model' in coronal equilibrium; their values for iron and oxygen are shown in Fig. 1. These two elements have radiation curves typical of light and medium mass impurities and demonstrate how the radiation peaks at low temperature . The result is that $\int_o^{T_1} (T)dT$ changes slowly once the peak is passed and eqn.(3a) then becomes insensitive to the upper limit of integration. The appendix gives values of $\int L(T)dT$ calculated from Post's data [9] and derives the following approximate relationship which is valid when $T \gtrsim 0.5$ keV for medium mass impurities, and $T \gtrsim 50$eV for light impurities.

$$\int_0^T L(T)dT \simeq 3.7 \times 10^{-36}\, T^{\frac{1}{2}}\, N^3 \text{ watt m}^3 \text{ keV} \qquad (4)$$

where the temperature T is in keV and N is the atomic number of the impurity ion.

Because L(T) peaks at low temperature the solution of eqn.(1) is $dT/dr \simeq$ constant until $T \lesssim 0.5$keV when radiation losses become

important and dT/dr changes rapidly; dT/dr tends to zero if all the power is radiated. Fig.2 illustrates this behaviour. It shows solutions of eqn.(1) for iron and oxygen impurities with dT/dr = 0 at T = 0 and κ_e,n_e and n_z assumed constant; also shown is L(T) against radius. The density used is $10^{20}m^{-3}$ and the other parameters chosen are appropriate to the reference parameters of INTOR as defined at the Workshop held in Vienna in February,1979 (see section 6). The value of dT/dr assumed at T = 2keV corresponds to 50MW being generated in the central plasma and then conducted to the peripheral plasma; this level of power is representative of both the alpha-particle power expected at ignition and the auxiliary heating power needed to reach ignition. The curves shown in Fig.2 are general and can be scaled to different plasma parameters since eqn.(1) may be re-written as

$$d^2T/d\alpha^2 = L(T) \qquad (5)$$

where $\alpha = r(n_e n_z/\kappa_e)^{\frac{1}{2}}$. Hence if dT/dr = o at T=0 then

$$\alpha/r = (n_e n_z/\kappa_e)^{\frac{1}{2}} = (Q_1/\kappa_e)\left[2\int_0^T L(T)dT\right]^{-\frac{1}{2}} = (dT/dr)_1\left[2\int_0^{T_1} L(T)dT\right]^{-\frac{1}{2}}$$

Fig.2 shows that most of the radiation comes from a narrow low temperature region, thus justifying the use of plane geometry in eqn.(1). For iron this region is about 3cm in width; for oxygen it is only millimetres wide and the assumption of coronal equilibrium will be poor.

Eqn.(2) implies that the onset of temperature profile collapse will be sudden as the radiated power increases. Consider the case where Q_1 is constant, then the integral may be expressed as

$$2\int_0^{T_1} \kappa_e\, n_e\, n_z\, L(T)dT = \gamma\, Q_1^2 \qquad (6)$$

Eqns.(2) and (6) give

$$Q_1^2 - Q_o^2 = \gamma Q_1^2 \tag{7}$$

and the fractional power radiated from the peripheral plasma is

$$(Q_1 - Q_o)/Q_1 = 1 - (1 - \gamma)^{\frac{1}{2}} \tag{8}$$

Eqn.(8) is plotted in Fig.3 and shows that the radiated power changes rapidly as $\gamma \to 1$ and temperature profile collapse becomes imminent. Consider the implications of eqn.(8). Suppose that n_z is determined by sputtering from the reactor walls. Initially n_z and γ will be small and little power is radiated. As n_z and hence γ increase the radiation will also increase causing the peripheral temperatures to fall, thus reducing the influx of sputtered impurities. As a consequence of this feed-back mechanism equilibrium is possible (e.g. see [10-12]). However eqn.(8) suggests that this equilibrium is sensitive to small changes of the integral in eqn.(6). For example, suppose that equilibrium is reached when the edge temperatures have fallen by a factor three, then two thirds of the power is radiated, $\gamma = 8/9$ and a 10% increase in the value of the integral will result in all the power being radiated thus making collapse imminent.

In short, once impurity radiation causes a substantial reduction in edge temperature, collapse is likely. It could be expected if an attempt were made to increase the plasma density by "gas-puffing" or if κ_e increased significantly. Now in a fusion reactor the initial aim is to achieve good energy confinement (i.e. small κ_e) so that the power required for ignition is small. However once ignition occurs the aim is to increase the power output which would normally entail increasing the plasma density and degrading the energy confinement. Both actions are liable to precipitate a collapse of the temperature profile if the peripheral plasma is already radiating a substantial fraction of the available power. Collapse could be avoided if the influx of impurities decreased and the impurities already present had time to escape.

The next section derives an estimate of the impurity density that will cause temperature profile collapse in a reactor.

3. THE PERIPHERAL IMPURITY LIMIT IN A REACTOR

The limiting impurity density at which self-sustained fusion becomes impossible is normally estimated by equating the alpha-heating power to the radiation loss from the central plasma,

thus $n_e^2 \langle\sigma v\rangle W_\alpha/4 = n_e n_z L(T)$

giving $n_z/n_e = \langle\sigma v\rangle W_\alpha/4L(T)$ (9)

where $\langle\sigma v\rangle$ = the mean fusion reaction rate

and W_α = the fusion energy per alpha particle = 3.5MeV.

Fig.4 shows n_z/n_e as a function of central temperatures for some typical impurities [4]. However the onset of temperature profile collapse sets an additional limit to the impurity density in the peripheral plasma which is now derived.

Consider the case when the impurities are concentrated in a peripheral region defined as $T \lesssim 2$keV. The thermal flux into this outer region is given approximately by

$$\left(\kappa_e dT/dr\right)_1 \simeq \int_o^{r_o} \frac{n^2}{4} \langle\sigma v\rangle W_\alpha \left(\frac{r}{r_o}\right) dr \qquad (10)$$

where r_o is the plasma radius at $T \simeq 0$.
Eqns.(10) and (^{3}a) determine the condition for temperature collapse. To get an estimate of the critical value of n_z assume that:

(i) n_e is constant throughout the plasma:
(ii) κ_e and n_z are constant in the peripheral region.

Under these assumptions eqn.(10) becomes

$$(\kappa_e dT/dr)_1 = n^2 \overline{\langle\sigma v\rangle} W_\alpha r_o/8 \qquad (11)$$

where $\overline{\langle\sigma v\rangle}$ is the fusion reaction rate averaged over the temperature profile. From eqns. (11) and (3) the permissible impurity concentration is given by

$$2\kappa_e(n_z/n_e)\int_o^{T_1} L(T)dT < \left[nr_o \overline{\langle\sigma v\rangle} W_\alpha/8\right]^2 \qquad (12)$$

which determines $\kappa_e(n_z/n_e)$ as a function of the mean temperature $\overline{T}$, nr_o and the impurity species. This result is only weakly dependent on the limit of integration. (see eqn.(4)).

Fig.5 shows contours of n_z/n_e in (nr_o,T) space for iron impurity with κ_e taken as the INTOR reference value and $\langle\sigma v\rangle$ averaged over a parabolic temperature profile.

To apply Fig.5 to a fusion reactor we need the ignition curve in (nr_o,T) space. Along this curve the alpha-power just balances the transport losses from the reacting central region. The ignition curve is given by

$$n^2 \overline{\langle\sigma v\rangle} W_\alpha/4 = 3nT/\tau_E \qquad (13)$$

where τ_E is the energy confinement time. The position and detailed shape of the ignition curve depend upon energy transport in the bulk plasma. For illustrative purposes Fig.5 shows the ignition curve for

$$\tau_E = 2\tau_{Ee} = 2\,(nr_o^2/4\kappa_e) = 10^{-20} nr_o^2 \qquad (14)$$

which is the INTOR reference value and is compatible with the value of κ_e used. It is important to note that the contours of n_z/n_e depend on the value of κ_e in the peripheral plasma whereas the ignition curve is determined by some average value of κ_e. The ignition curve shown assumes that κ_e is constant throughout the plasma whereas it has been suggested that $\kappa_e \propto T^{-1}$ for $T \gtrsim 1$keV [13,14].

On the assumption that κ_e is constant eqns.(12), (13) and (14) determine the critical impurity concentration for temperature profile collapse namely

$$n_z/n_e = \frac{3\overline{T}\langle\overline{\sigma v}\rangle W_\alpha}{16\int_o^{T_1} L(T)\,dT} \qquad (15)$$

which is independent of κ_e.

Fig.6 shows eqn.(15) for a parabolic temperature profile plotted for several impurities using values for $\int_o^{T_1} L(T)dT$ taken from the appendix; it should be compared with Fig.4 which shows limiting impurity concentrations for the central region. The actual values are similar and within the uncertainties of the assumptions are essentially the same. The relative importance of impurity radiation from the peripheral and central regions is likely to be determined by the profile of n_z which, under the influence of neoclassical transport is not expected to be uniform; this point is considered in section 5.

The next section applies the expressions obtained in sections 2 and 3 to considerations of thermal stability in a self-sustained fusion reactor when all the fusion power is radiated.

4.THERMAL STABILITY OF A RADIATION-COOLED FUSION REACTOR

Fig.7 shows the ignition curve defined by eqns.(13) and (14). Along this curve the plasma losses balance the alpha-heating power and equilibrium exists; however this equilibrium is not necessarily stable. If r_o is constant points on the curve to the right of the minimum are stable while those on the left are unstable. The reason for this result is simple to see. Above the curve the alpha power exceeds the losses and the temperature increases, while below the curve the plasma cools. Hence above the ignition curve the plasma heats up until the right-hand side is reached. If the plasma lies below the ignition curve, but above the minimum value of nr_o, then the temperature either falls to zero or to the right-hand side depending upon the initial temperature. Illustrative trajectories are shown in Fig.7. The unstable nature of the equilibrium leads to a severe

control problem for fusion reactors [15-18] particularly as the desired operating point of $\overline{T}_i \simeq$ 10keV is expected to lie on the unstable side of the ignition curve. Several authors have considered the thermal stability of fusion reactors and schemes for obtaining stable operation e.g. see [19-25].

The trajectories shown in Fig.7 assume that the plasma radius is constant; this will be the case if the point $T \simeq 0$ is determined physically by a limiter or divertor separatrix. However if the plasma is entirely radiation-cooled then the point $T \simeq 0$ is free to move and the trajectories in Fig.7 no longer apply.

The trajectories for a radiation-cooled reactor can be estimated as follows. Assume that all the radiation comes from the peripheral region, then the energy flux conducted into this region is given by

$$\frac{3}{2} n (\overline{T}_e + \overline{T}_i) \frac{\pi r_o^2}{\tau_E} \simeq 2\pi r_o \kappa_e \frac{dT_e}{dr} \qquad (16)$$

With $\overline{T}_e = \overline{T}_i$ eqns.(3), (14) and (16) give

$$\frac{n r_o}{\kappa_e^{\frac{1}{2}}} = 3\overline{T} \left[2 \frac{n_z}{n} \int_o^{T_1} L(T) dT \right]^{-\frac{1}{2}} \qquad (17)$$

If the impurity fraction n_z/n is constant then nr_o varies as $\overline{T}$. Hence if the alpha-heating power exceeds the losses, so that $\overline{T}$ increases, then the plasma radius r_o increases until it is constrained by the machine boundary; conversely if the losses exceed the heating power then the plasma cools and shrinks. The trajectories defined by eqn.(17) are shown in Fig.8. The entire ignition curve is now unstable apart possibly for the regions at either end corresponding to high density and either high or low temperature; these regions are probably of no practical importance.

The change in character of the thermal instability that occurs when a fusion reactor radiates all its power adds to the problem of

control and could render impractical schemes involving the deliberate addition of impurities [23].

5. THE EFFECT OF NEOCLASSICAL IMPURITY TRANSPORT ON PERIPHERAL RADIATION

For simplicity n_z has been assumed constant in the preceding sections; this assumption is not justified if neoclassical transport dominates anomalous transport. Throughout the peripheral plasma ($T \lesssim 2$keV) impurities are typically in the Pfirsch-Schlüter regime of neoclassical theory while the hydrogen ions are collisionless except at the extreme edge where $T \lesssim 200$eV. It will be shown later that the behaviour of the impurities in the extreme edge, when both impurities and hydrogen ions are collisional, has a marked effect on impurity radiation but for the present we consider the effect of assuming that the hydrogen ions are collisionless everywhere. Then if impurity-on-impurity collisions are ignored the impurity flux may be written as

$$\Gamma_z = -D_{AN} \frac{dn_z}{dr} + D_o \left\{ \langle Z \rangle \frac{n_z}{n_H} \frac{dn_H}{dr} - \frac{dn_z}{dr} - \left(\frac{\langle Z \rangle}{2} + 1 \right) \frac{n_z}{T} \frac{dT}{dr} \right\} \qquad (18)$$

where D_{AN} is the anomalous plasma diffusivity used to describe the transport of n_e:

$D_o = \rho_H^2 q^2 / \tau_H$:

ρ_H is the hydrogen ion-gyro radius :

q is the safety factor:

τ_H is the hydrogen collision frequency :

$\langle Z \rangle$ is the mean charge state of the impurity ions.

Eqn.(18) is the standard expression for impurity diffusion (e.g. see [26]) with an anomalous term $D_{AN}\, dn_z/dr$ added. The addition of this term is a commonly used recipe (e.g. see [12,27]); justification for its inclusion is discussed in refs.[28,29].

Eqn.(18) can be used to estimate the equilibrium impurity profile in the peripheral plasma. Assume that the hydrogen scale length is much longer than the temperature scale length in the region of interest (this assumption is supported by the computer modelling described in section 6). Hence $n_H^{-1} dn_H/dr << T^{-1} dT/dr$ and in equilibrium, when $\Gamma_z = 0$, eqn.(18) becomes

$$(D_{AN} + D_O) \frac{1}{n_z} \frac{dn_z}{dr} \simeq -D_o \, (<Z>/2+1) \frac{1}{T} \frac{dT}{dr} \qquad (19)$$

which integrates to give the general expression

$$n_z = n_{zo} \exp \left\{ - \int_{T_o}^{T} \frac{(<Z>/2+1)}{1+D_{AN}/D_O} \frac{dT}{T} \right\} \qquad (20)$$

where n_{zo} is the impurity density at T_o. Fig.9a shows solutions of eqn.(20) for iron impurity in INTOR.

The average charge state <Z> was determined as a function of T from the average ion model [9]. The INTOR reference value for D_{AN} was used

$$\text{i.e.} \quad D_{AN} = \chi_e/4 = \kappa_e/4n_e = 1.25 \times 10^{19} n_e^{-1} m^2 sec^{-1} \qquad (21)$$

n_e was assumed constant and the lower limit of integration was taken as 20eV.

From Fig.9a it is apparent that 'temperature screening', caused by the dT/dr term in eqn.(18), is a strong function of n_e; this is because $D_{AN}/D_O \propto n^{-2}$ and appears in the exponential term of eqn.(20). Physically what happens is that at low densities, where $D_{AN} >> D_O$, the anomalous transport swamps the neoclassical effects and the n_z-profile tends to flatten. However at high densities, where $D_{AN} << D_O$, the dT/dr term in eqn.(19) causes strong outward transport of the impurities. The screening term becomes increasingly important at low temperature since

$$D_O(<Z>/2+1) \frac{n_z}{T} \frac{dT}{dr} \propto n_H \, n_z \, (<Z>/2+1) \frac{1}{T^{3/2}} \frac{dT}{dr}$$

and dT/dr is essentially constant until T ≃ 100eV where the radiation from iron becomes large (see Fig.2).

Since n_z as a function of T has been determined $n_z(T)L(T)$ and its integral can be evaluated. The integral is of particular interest since $\int_o^T n_e n_z(T)L(T)dT$ determines the collapse condition (see eqn.(2a)). Figs.9b and 9c show $n_z(T)L(T)$ and its integral for iron with n_e as a parameter. Note that when $n \gtrsim 0.5 \times 10^{20} m^{-3}$ neoclassical effects become important and 'temperature screening' causes n_z to decrease rapidly as T increases thus reducing the value of $\int_o^T n_z L(T)dT$ and making it tend to zero at high densities. This result implies that 'temperature screening' can markedly reduce impurity radiation. However the curves in Fig.9 were obtained on the assumption that the hydrogen ions were everywhere collisionless. This assumption is not justified when $T \lesssim 200eV$. The change in neoclassical impurity transport as the hydrogen becomes collisional can have a profound effect on the peripheral impurity radiation and is considered next.

The hydrogen ions become collisional when

$$Rq/\tau_H v_H \gtrsim 1 \qquad (22)$$

where v_H is the thermal velocity of the hydrogen ions. Eqn.(22) can be rewritten as

$$T \lesssim 80\ (n_{20} a\ q/\varepsilon)^{\frac{1}{2}}\ eV \qquad (23)$$

where n_{20} is the plasma density in units of $10^{20} m^{-3}$ and $\varepsilon = a/R$. For a Tokamak Reactor $n_{20}a \simeq 1$, $q \simeq 3$, $\varepsilon \simeq \frac{1}{3}$ and eqn.(23) becomes $T \lesssim 200eV$. Hence eqn.(18), and thus eqn.(20), are invalid at low temperature. Rutherford [30] considered the situation when both hydrogen and impurity ions were collisional and concluded that the dT/dr term as well as the dn/dr term would give inward diffusion of the impurities; namely that there would be no

'temperature screening'. Since impurity radiation typically peaks in the range T ≈ 30 - 100eV this reversal of the dT/dr term when $T \lesssim 200$eV has a marked effect on impurity radiation.

Samain and Werkoff [31] have analysed the transition case. Their general result reduces to the results obtained by Rutherford [30] and Hirshman [26] in the appropriate limits. Samain and Werkoff's expression for impurity flux is

$$\Gamma_z = D_0 \left\{ K\left(Z \frac{n_z}{n_H} \frac{dn_H}{dr} - \frac{dn_z}{dr} \right) + \frac{H[Z + O(1)] n_z}{T} \frac{dT}{dr} \right\} \qquad (24)$$

where K and H are functions of $Rq/v_H\tau_H$ and $Z^2 n_z/n_H$. As the hydrogen ions become collisionless $H \to -0.5$ and $K \to 1$ thus tending to Hirshman's [26] result (see eqn.(18)). When the hydrogen ions are strongly collisional H changes sign while $K \simeq 1$. The transition occurs near $Rq/v_H\tau_H = 1$.

The reversal in sign of the dT/dr term changes the n_z-profile and the power radiated. These changes were estimated by repeating the analysis leading to Fig.9 using eqn.(24), with the anomalous term added, in place of eqn.(18). The example given by Samain and Werkoff was used to obtain values for K and H through the transition region and the term O(1) was dropped. Fig.10 shows the result and should be compared with Fig.9 where 'temperature screening' was retained at low temperatures.

Comparing Figs.9a and 10a shows that when $n_e \lesssim 0.5 \times 10^{20} m^{-3}$ both n_z-profiles tend to be flat since $D_{AN} >> D_0$ and anomalous transport dominates. However at higher densities the behaviour of n_z is different In Fig.9a n_z continually decreases with increasing temperature. By contrast in Fig10a n_z initially increases until it reaches a maximum at T ≈ 100eV where the dT/dr term changes sign. Figs.10b and 10c show $n_z(T)L(T)$ and its integral; they should be compared with Figs.9b and 9c. The result of the change in n_z-profile is that the integral now increases as n_e increases. This happens because n_z peaks in the temperature region where impurity radiation is at a maximum. The examples shown have assumed constant plasma density. In practice the dn_H/dr

term in eqn.(24) can be expected to enhance the peak in n_z. The net result is that when $D_{AN} < D_0$ at $T \simeq 100eV$ impurities tend to accumulate in a temperature range where they radiate strongly. This point is considered further in section 8 where the density limits in current tokamak experiments are discussed.

The impurity radiation from the peripheral plasma is dependent upon the details of impurity transport and the resulting n_z-profile. Transport theory in this region is particularly complex and little experimental evidence concerning the behaviour of n_z exists. The idealized analysis presented is only indicative of the behaviour that can be expected. The effect of relaxing some of the simplifying assumptions made is examined in section 7 where the peripheral radiation from INTOR is modelled using a 1-D diffusion code. The next section describes the model used in these computations.

6. COMPUTER MODEL OF THE PERIPHERAL RADIATION FROM INTOR

The computer model uses the 1-D tokamak diffusion code HERMES [32]. The model is relatively simple and is representative of the diffusion models currently used to describe conceptual reactors and large tokamaks.

The Machine

INTOR dimensions and machine parameters are used.

Major radius	$R = 4.5m.$
Equivalent minor radius	$a = 1.5m.$
Toroidal current	$I = 4MA.$
Toroidal magnetic field	$B_\phi = 5$ tesla.

An atomic mass of 2.5 is used to simulate a DT-mixture.

Plasma Transport

The INTOR reference transport is used.

Electron thermal diffusivity $\chi_e = \kappa_e/n_e = 5\times10^{19}/n_e m^2 sec^{-1}$ [Bohm if $q \lesssim 1$]

Ion thermal diffusivity	χ_i = 3x(the neoclassical value)
Plasma diffusivity	$D = \chi_e/4$ + neoclassical transport including the Ware Effect.

Impurity Transport

The impurity modelled is iron assumed to be in the Pfirsch-Schlüter regime. Hence, except at low temperatures, eqn.(18) is used with an additional term describing impurity-on-impurity collisions. At low temperatures, where the hydrogen becomes collisional, the results of Samain and Wekoff [31] are approximated by the following prescription. When $\nu_o = Rq/\tau_H v_H > \frac{1}{2}$ the dT/dr term is reduced by $(2\nu_o)^{-1}$. Since $\nu_o^{-1} \propto T^2$ this prescription rapidly switches off the 'temperature screening' term close to the point predicted by Samain and Werkoff. This procedure is similar to that used by the TFR Group [28] only they choose to put the dT/dr term to zero at the plasma edge. Their procedure is appropriate if the computational cell at the edge is the only one at low temperature; it is inappropriate if the temperature profile collapses since further cells fall to low temperature.

The prescription used does not give the reversal in sign predicted by Samain and Werkoff but it does prevent the dT/dr term from becoming anomalously large at low temperature. It underestimates any peaking in n_z at low temperatures due to neoclassical transport.

Impurity Source

The level of impurities is set by one of two methods. In some computations the boundary value of n_z is made non-zero which fixes the impurity density at the plasma edge; the density within the plasma then follows from the transport equation. The boundary value of n_z can be viewed as the impurity density in the shadow of a limiter or at the separatrix of a divertor.

Alternatively the boundary value is set to zero and an impurity flux due to the sputtering of iron by neutral deuterium and tritium is modelled. The value of the sputtering co-efficient and its dependence on neutral energy is taken from experimental results compiled by

Bohdansky et al and quoted in ref.[33]. The sputtered iron atoms are assumed to have an energy of 5eV and are deposited within the plasma by using the ionization rate to give an e-folding distance. In practice this procedure normally results in the iron atoms being deposited in the first computational cell which has a width of 3.75cm (40 equal width cells in 1.5m).

Neutral Hydrogen

An influx of neutral DT-mixture into the plasma is modelled. The atoms are arbitrarily given an energy of 30eV and transported and deposited within the plasma using a Monte Carlo method [34]. Normally the flux is continually adjusted so that ionization just balances the loss of hydrogen by diffusion, (i.e. a recyling co-efficient of unity). In some cases the recycling co-efficient is made greater than unity to simulate an increase in density by 'gas-puffing',

Power Sources

Power released by fusion reactions is omitted. Instead a source of 50MW is given to the electrons on axis. The magnitude of this source is roughly the beam power required to ignite INTOR and is also close to the alpha-power produced at ignition. Since the essential physics involved with temperature profile collapse occurs in the peripheral plasma the central assumptions are largely irrelevant once the power transported from the central region is determined. To include thermonuclear power would make the model needlessly complex and obscure since the reaction rate is a strong function of density and temperature.

Ohmic heating power is included in the model although it is small (< 1MW).

Impurity Radiation

As in the previous analysis Post's average ion coronal model [4] is used to give L(T). Since iron is the impurity modelled the value of $\int_{T=20eV}^{T=2keV} L(T)dT$ is approximately 10^{-31} watt m^3 keV. (see appendix 1). This is the appropriate value to use when applying the

formulae of section 2 to the results that follow in section 7.

Because L(T) changes rapidly at low temperatures (see Fig.1) a small computational cell width is needed to give adequate resolution and avoid numerical problems. In the computations that follow the radius was divided into 40 equal cells but when T_e<2keV the cells were further sub-divided into smaller units to determine the mean power radiated per cell.

7. COMPUTATIONAL RESULTS FROM MODELLING PERIPHERAL RADIATION IN INTOR

This section presents results obtained using the computer model described in section 6; they check and extend the analysis in the previous sections.

Equilibrium profiles when temperature collapse is imminent

The impurity density at which the radiation loss equals input power was determined at several plasma densities by changing the boundary value of n_z. Fig.11a shows profiles of T_e, n_e and n_z at three densities. In each case dT/dr = 0 at the plasma boundary; hence the entire input power of 50MW is radiated and temperature profile collapse is imminent.

The impurity densities in the three cases agree well with the values given by eqn.(3). If the mean electron density is substituted in eqn.(3) the following values for n_z are obtained: $6.3 \times 10^{17} m^{-3}$, $4.3 \times 10^{17} m^{-3}$ and $2.2 \times 10^{17} m^{-3}$. The ratios of these values to the peak values of n_z in Fig.11a are 1.4, 1.3 and 1.0. The systematic trend in these ratios results from changes in the profile of n_e which becomes flatter as density is increased.

In section 4 it was argued that neoclassical effects would cause impurities to accumulate at the plasma edge if $n \gtrsim 0.5 \times 10^{20} m^{-3}$ so that $D_0 \gtrsim D_{AN}$. The profiles in Fig.11a confirm this prediction. The impurity density is essentially constant at low plasma density whereas the n_z-profile becomes hollow at high density. In the computer model the reversal in sign of the dT/dr term in the impurity transport equation is not included; therefore the initial

increase in n_z at the plasma boundary is caused by the dn_H/dr term which was omitted in the derivation of eqn.(20). Fig.11a shows that this omission is not justified in the extreme edge region where $dT/dr \simeq 0$. Elsewhere the temperature scale length is much shorter than the density scale length (i.e.$T^{-1}dT/dr >> n^{-1}dn/dr$) thus justifying the omission of the dn/dt term in the derivation of eqn.(20).

The effect of sputtering by neutrals

Fig.11b shows the three cases in Fig. 11a repeated with the boundary value of n_z set to zero and sputtering by neutral DT included. At the lowest plasma density the impurity density, resulting from sputtering, is within a factor two of the critical value but only 11.7MW is radiated and the temperature profile is hardly affected. In contrast at the highest density n_z is close to the critical value, 44.1MW is radiated and the temperature profile is noticeably flattened at the plasma's edge. These results are in accord with the arguments in section 2 (see Fig.3).

An important point to note is that for typical INTOR parameters neutral sputtering of iron alone is sufficient to bring the temperature profile close to collapse. The inclusion in the model of charged-particle sputtering, sputtering due to impurities and the desorption of light impurities such as oxygen would exacerbate the situation.

Temperature collapse caused by increasing $\kappa_e n_e n_z/Q^2$

Eqn.(3) predicts that temperature profile collapse will occur when $\kappa_e n_e n_z/Q^2$ exceeds a critical value. Starting from the medium density equilibrium shown in Fig.11a collapse was induced by increasing the boundary value of n_z from $3 \times 10^{17} m^{-3}$ to $5 \times 10^{17} m^{-3}$. Collapse was also caused by reducing the input power from 50MW to 40MW. In both cases the $T \simeq 0$ point moved inwards about 30cm in roughly 1 sec. A new equilibrium was approached as Q gradually increased, due to cylindrical geometry, and the profiles of n_e and n_z changed.

The collapse associated with an increase in n_e is of most

practical interest since, in a reactor, the plasma density must be controlled and changed to optimise the heating phase before ignition and the power output after ignition. Fig.12 shows the effect on the medium density equilibrium of increasing the recycling co-efficient from unity to 1.1. This increase in recycling co-efficient causes the density to slowly rise and simulates increasing plasma density by 'gas-puffing' or by low velocity injection of D-T pellets.

Fig.12 shows that the $T \simeq 0$ point moves inwards about 40cm in 1.4 sec. at which time the collapse is slowing down. The dT/dr term in the impurity transport equation causes n_z in the central plasma to slowly decrease as n_e increases and changes the ratio D_o/D_{AN}. The peaking of n_z near the $T \simeq 0$ point results from the dn_H/dr term in the region where $T \simeq 0$ and the dT/dr term when $T \gtrsim 200$eV. A secondary effect is apparent from Fig.12. As the temperature profile collapses the neutral hydrogen injected at the plasma boundary penetrates further before being ionized since the temperature in the collapsed region is leV or less. As a consequence the profile of n_e changes and peaks in the radiating region where dT/dr changes rapidly; this effect tends to increase the radiated power.

Fig.13 shows a faster collapse caused by making the recycling co-efficient 1.2; this corresponds to doubling the density in roughly two energy confinement times. The peaking in n_z is more pronounced than in Fig.12 since higher densities are reached and the ratio $D_o/D_{AN} \propto n^2$ is larger giving stronger neoclassical effects.

Fig.14 shows an even more extreme case of collapse. Again the recycling co-efficient is 1.2 but the plasma current is now 2MA instead of 4MA. This change in current increases q by a factor two which changes the ratio of D_o/D_{AN} by a factor four thus further enhancing neoclassical effects.

The effect of the dT/dr term as $T \to 0$

Figs.9 and 10 of section 5 show how the profile of n_z is affected if 'temperature screening' is retained as $T \to 0$. Maintaining

outward transport driven by dT/dr in the region where the hydrogen ions are collisional drastically changes the impurity density profile and the resulting impurity radiation. This change in behaviour is shown by the computer model. Fig.15 shows the time evolution of profiles, for the case illustrated in Fig.12, when eqn.(18) is used for impurity transport at all temperatures so that the dT/dr no longer tends to zero as the hydrogen ions become collisional. This minor change in impurity transport has a marked effect on the profiles of n_z and T_e. The decrease in central values of n_z is much greater than before and a sustained collapse in the temperature profile no longer occurs. Instead a new equilibrium is quickly established with a narrow low temperature region at the plasma edge. There is, of course, no justification for using eqn.(18) as $T \to 0$ other than simplicity of the computer model.

8. DENSITY LIMITS IN CURRENT TOKAMAK EXPERIMENTS

Several authors[5 - 8] have suggested that the disruptive instabilities observed in current tokamak experiments may be caused by a decrease in edge temperature due to peripheral radiation. Sykes and Wesson [35] have shown theoretically by numerical simulation that disruptions can be caused by edge-cooling. Apgar et al [36] argue that the density limit observed in ALCATOR results from shrinkage of the current channel brought about by cooling near the plasma boundary by impurity radiation. If we make the assumption that edge-cooling will lead to a disruption then eqn.(3a), which is the condition for temperature profile collapse, will also be the condition for the onset of disruptive instability. On the basis of this assumption eqn.(3a) can be used to derive an expression for the density limit of an ohmically-heated tokamak which is consistent with the experimentally observed limits (e.g. see refs.[6,37,38]). The expression is now derived.

The heat flux near the boundary of an ohmically-heated tokamak may be written as:

$$Q = VI/(2\pi R \times 2\pi a) \simeq \kappa_e \overline{T}/a \qquad (25)$$

where V is the voltage drop,

I is the current,

$\overline{T}$ is the mean temperature.

The voltage is given by

$$V = I(2R\eta/a^2) \qquad (26)$$

where η is the classical Spitzer-Harm resistivity [39] given by Hinton and Hazeltine [40] namely,

$$\eta = \frac{ne^2}{m_e \tau_e} \gamma(Z_{eff}) = \eta_o \gamma(Z_{eff}) \qquad (27)$$

where $$\gamma(Z_{eff}) = Z_{eff}[.29 + 0.46/(1.08 + Z_{eff})] \qquad (28)$$

and $$Z_{eff} = (n_H + Z^2 n_z)/n_e = 1 + (Z^2 - Z)n_z/n_e \qquad (29)$$

Eqns.(25) and (26) with (3a)give

$$\left(\frac{I}{2\pi n_e a^2}\right)^2 \eta\overline{T} < \frac{n_z}{n_e}\int_0^T L(T)dT \qquad (30)$$

which is the condition for the onset of temperature profile collapse. (Note that this result is independent of κ_e.) Eqn.(29) may be used to express n_z/n_e in terms of Z_{eff} giving:-

$$\left(\frac{I}{2\pi n_e a^2}\right)^2 \eta_o \overline{T} < \left[\frac{Z_{eff}-1}{\gamma(Z_{eff})}\right](Z^2-Z)^{-1}\int_0^1 L(T)dT \qquad (31)$$

The current is related to the safety factor q by

$$q = \frac{2\pi}{\mu o}\frac{B}{I}\frac{a^2}{R} \qquad (32)$$

and $\int_0^1 L(T)dT$ can be evaluated by eqn.(4) to give

$$q^{-1} < 3.5 \times 10^{-22} \frac{R\, n_e}{B} \left[\frac{(Z_{eff}-1)}{\gamma(Z_{eff})} \frac{N^3\, \bar{T}}{(Z^2-Z)}\right]^{\frac{1}{2}} \qquad (33)$$

where R, B and n_e are in S.I.units and T is in eV.
For fully stripped light impurities such as carbon, nitrogen and oxygen $[N^3/(Z^2-Z)]^{\frac{1}{2}} \simeq 3$ and eqn.(33) becomes

$$q^{-1} < 10^{-21} \frac{R\, n_e}{B} \left[\frac{Z_{eff}-1}{\gamma(Z_{eff})}\right]^{\frac{1}{2}} \bar{T}^{\frac{1}{2}} \qquad (34)$$

This expression is in rough agreement with the empirical limit found by Murakami et al [6] if we assume that $q \simeq 3$, $\bar{T} \simeq 300$eV and $Z_{eff} \simeq 1.5$.

The value of $\bar{T}^{\frac{1}{2}}$ in eqn.(34) can be estimated by equating the ohmic power to the plasma losses

$$\text{i.e.} \quad I^2\eta\, 2R/a = 2\pi R \pi a^2 3n\bar{T}/\tau_E \qquad (35)$$

and assuming 'Alcator scaling' so that

$$\tau_E = 10^{-20} n a^2 \qquad (36)$$

After some manipulation eqn.(34) becomes

$$q^{-1} < 1.6 \times 10^{-39} \left\{\frac{R\, n_e}{B}\left(B\, \frac{a}{R}\right)^{2/5}\right\}^2 F(Z_{eff}) \qquad (37)$$

where $F(Z_{eff}) = (Z_{eff} - 1)\,[\gamma(Z_{eff})]^{-3/5}$

$$\simeq (Z_{eff} - 1)\left\{Z_{eff}\left[.29 + .46/(1.08 + Z_{eff})\right]\right\}^{-3/5} \qquad (38)$$

Fig.16 shows the density limit given by eqn.(37) for four values of Z_{eff}. Also shown are experimental points taken from the tokamak results compiled by Pfeiffer and Waltz [41]. (Results for helium operation are omitted). In assessing the significance of Fig.16 two points should be noted. Firstly, for most of the experimental points no attempt was made to reach maximum density. Secondly, the values of Z_{eff} given in ref.[41] are estimated from assumed temperature and density profiles; in consequence the uncertainty of Z_{eff} can be

large particularly at values near unity.

Fig.17 illustrates data from the DITE tokamak [42] plotted in $(q^{-1}, n_e R/B)$ space showing the observed density limits for different values of Z_{eff}. For comparison eqn.(34) is also plotted for Z_{eff} = 1.5, 2 and 6 on the assumption that the mean temperature is 300eV.

Figs. 16 and 17 exhibit good agreement between theory and experiment and strongly suggest that peripheral radiation does indeed limit the density in ohmic-heated tokamaks. At first sight the agreement seems surprisingly good for such a simple analysis. However it should be noted that n_z is described by Z_{eff} which is a measured parameter. Hence no assumptions about the impurity source or magnitude are made. In addition eqn.(34) is independent of κ_e; thermal transport enters through eqn.(36) and only weakly influences the final result. Finally eqn.(34) depends on the square root of $\int_o^T L(T)dT$ thus decreasing the dependence of the result on the details of the radiation physics.

The analysis does not explain why the limiting value of n_e decreases at $q^{-1} \simeq 0.2$ as seen in Fig.17. A possible explanation is that at this value of q sputtering of wall material commences. This explanation is supported by the following argument. Eqns. 32, 35 and 36 determine the mean temperature; for DITE it is about 200eV when $q^{-1} = 0.2 - 0.3$. The energy of escaping neutrals is typically about half the mean temperature giving a neutral energy of $\sim$ 100eV which is close to sputtering threshold for hydrogen atoms on stainless steel.

Fig.18 shows further results from DITE [37]. The toroidal magnetic field was kept constant at 1.35 tesla and the limiting density was determined at different q-values with and without neutral beam heating. With auxiliary heating the density limit for ohmic heating alone can be passed. This result is consistent with the arguments already presented since the limit derived depends on equating the peripheral radiation to the ohmic-heating power; with an additional power source more radiation can be tolerated before the temperature profile collapses. However a new density limit is encountered with neutral-beam heating

as shown in Fig.18. We now consider its possible cause.

Engelhardt et al.[43] attribute the density limit in PULSATOR to impurity accumulation occuring on axis when neoclassical impurity transport dominates anomalous transport. This suggestion is similar to the point covered in sections 5 and 7 where it was shown that impurity accumulation at the edge begins to appear when $D_O/D_{AN}>1$. If the INTOR reference value for D_{AN} is used, this inequality becomes

$$D_O/D_{AN} = 6 \times 10^{-40}(nq/B)^2 T_e^{-\frac{1}{2}} > 1 \qquad (39)$$

or

$$2.5 \times 10^{-20}(nq/B)T_e^{-\frac{1}{4}} > 1 \qquad (39a)$$

Impurity radiation from light impurities is only important at low temperatures and in any case eqn.(39a) is insensitive to the value of temperature chosen; we therefore take T_e = 100eV to give

$$nq/B = 1.3 \times 10^{20} m^{-3} T^{-1} \qquad (40)$$

This line is shown in Fig.19 and compared with the DITE density limits in Fig.18. Also shown is the ohmic-heating limit given by eqn.(37). The experimental density limit with neutral beam heating occurs at values of q about a factor two larger than those predicted by eqn.(40). Hence at the density limit D_O exceeds D_{AN} by a factor of approximately four (since $D_O \propto q^2$) and marked impurity accumulation due to neoclassical effects can be expected. It is tempting to speculate that the density limit observed with neutral beam heating results from a collapse of the temperature profile which occurs when neoclassical transport dominates anamalous transport thus causing the impurities to accumulate.

The accumulation referred to is in the peripheral plasma where $T \lesssim 200$eV. Impurities are transported into this region by dT/dr and then retained there by dn_H/dr; the dT/dr term will also retain the impurities since it changes sign as the hydrogen ions become collisional. If this explanation for the beam-heating limit is correct then it will be independent of the heating method used and the impurities involved. It does depend on assuming an expression for the anomalous diffusivity of impurities in the peripheral plasma about which little is known. On the other hand as long as $D_{AN} \propto n^{-1}$ the constant of proportionality could be changed by a factor two or more without affecting the argument.

9. DISCUSSION AND CONCLUSIONS

Although peripheral radiation and its effect on Tokamak Reactors has been discussed this can only be done within the framework of present knowledge. The paper does not necessarily predict what will happen in a Tokamak Reactor; there is insufficient experimental information and theoretical understanding to make such predictions with any degree of confidence. It should be viewed as an examination of the consequences to reactors of the physics currently assumed to apply in tokamaks and modelled by 1-D diffusion codes. Hopefully these codes give some indication of what will happen in a reactor-sized tokamak.

The question of the impurity source and the way it is coupled to the plasma parameters has been largely ignored. The conditions in which the impurity influx can adjust itself to give a cold stable edge region, as assumed in refs. [10,11,12], have not been considered. The fact that the analysis predicts a density limit for ohmic-heated tokamak that is consistent with current experiments suggests that a cold stable edge region is not normal behaviour in present machines. However current tokamaks are usually limited in the discharge time available to them. There is the possibility that temperature profile collapse induced by increasing the density could be avoided if the rate of increase in density was sufficiently small. Then, if the influx of impurities decreased as the edge cooled, those impurities already present would have time to escape. This would require a density doubling time of many energy confinement times.

The derivation of the density limit assumes that temperature profile collapse will inevitably lead to disruption irrespective of the value of q at the plasma boundary. This assumption is rather sweeping. The work of Sykes and Wesson [35] suggests that disruption is likely when the $T \simeq 0$ surface approaches the $q=2$ surface. If this is correct then operation with a stable low temperature edge region would be favoured by high-q; however strong neoclassical effects would be expected since $D_0 \propto q^2$.

The values for the radiation term L(T) have been taken from results obtained by assuming coronal equilibrium. This assumption is poor particularly for light impurities. However even if L(T) is considerably different under conditions of non-coronal equilibrium it is not obvious to what extent $\int^{T} L(T)dT$ will be different. The fact that the density limit for ohmic-heated tokamaks is close to the predicted limit suggests that the integral is correct to within an order of magnitude. Note that the density limit involves the square root of the integral.

The results obtained depend on the transport assumed for the peripheral plasma; a region where measurement is particularly difficult. Ideally what is needed to minimize peripheral radiation is a small thermal diffusivity and a large particle diffusivity; these two requirements are in conflict.

It might be thought that if neoclassical transport of impurities occurs then 'temperature screening', or the outward transport of impurities due to dT/dr, would mitigate the effect of inward transport due to dn/dr. This appears not to be the case. Because the dT/dr term changes sign as the hydrogen ions become collisional impurities tend to accumulate in the low temperature edge region where they radiate strongly.

As far as the implications for Tokamak Reactors are concerned it is concluded that peripheral radiation is likely to impose more severe constraints than radiation from the central plasma; if neoclassical transport of impurities pertains then the central impurity density will be considerably smaller than that near the edge. The peripheral radiation depends on plasma transport and its behaviour in practice is likely to be complex. The problem of exercising satisfactory control over a self-sustained Tokamak Reactor can be expected to increase substantially if it becomes predominantly radiation-cooled.

APPENDIX

Section 2 of the paper points out the importance of the integral $\int_o^T L(T)dT$ in determing the effect of peripheral radiation. Post et al [9] calculate L(T) for about 40 elements on the basis of an 'average ion model' in coronal equilibrium. This data has been used to evaluate the integral for each element. The results are given below.

Fig.A1 shows how the integral varies with the upper limit of integration for several common impurities. The main point to notice is that after an initial rapid change the value of the integral increases slowly with temperature; in this region the value of the integral is insensitive to the upper limit of integration.

Fig.A2 shows the value of the integral for a number of elements as a function of atomic number N when the upper limit of integration is 10keV. The points approximate closely to an N^3 law. Fig.A3 shows a similar plot with the upper limit of integration taken as 1keV. In this case all but the heavy elements fit an N^3 law. If the temperature taken for the upper limit of integration is sufficient to ionize light impurities to helium-type ions and medium mass impurities to neon-type ions then the integral is given approximately by

$$\int_o^T L(T)dT = 3.7 \times 10^{-36} T^{\frac{1}{2}} N^3 \text{ watt m}^3 \text{ keV}$$

In practice this expression is valid when T > 0.5keV for medium mass impurities and when T > 50eV for light impurities.

ACKNOWLEDGEMENT

The authors thank Dr. D.E.Post for supplying a magnetic tape of the radiation data used in this study.

REFERENCES

[1] MEADE, D., Nucl.Fusion 14, (1974) 289.

[2] CONN, R.W and KESNER, J., Nucl.Fusion 15, (1975) 775.

[3] STACEY, Jr., W.M., BERTONCINI, P.J., BROOKS, J.N. and EVANS, Jr., K., Nucl.Fusion 16, (1976) 211.

[4] JENSEN, R.V., POST, D.E. and JASSBY, D.L., Critical Impurity Concentrations for Power Multiplication in Beam-Heated Toroidal Fusion Reactors . Princeton Plasma Physics Lab.Report . PPPL-1350(1977).

[5] VERSHKOV, V.A. and MIRNOV, S.V., Nucl.Fusion 14,(1974) 383.

[6] MURAKAMI, M., CALLEN, J.D. and BERRY, L.A., Nucl.Fusion. 16, (1976) 347.

[7] GIBSON, A., Nucl.Fusion 16, (1976) 546.

[8] REBUT, P.H. and GREEN, B.J., in Plasma Physics and Controlled Nuclear Fusion Research (Proc.6th Int.Conf.Berchtesgaden 1976) Vol II IAEA, Vienna (1977) 3.

[9] POST, D.E., JENSEN, R.V. TARTAR, C.B.GRASBERGER, W.H. and LOKKE, W.A. Atomic Data and Nuclear Data Tables. 20, No.5, (1977) 397.

[10] GIBSON, A. and WATKINS, M.L., in Controlled Fusion and Plasma Physics (Proc.8th Eur.Conf.Prague,1977) 1, (1977) 31.

[11] WATKINS, M.L. and GIBSON, A., in Controlled Fusion and Plasma Physics (Proc.9th Eur.Conf., Oxford 1979) 1, (1979) 164.

[12] WATKINS, M.L., STRINGER, T.E., GIBSON, A., CORE, W.G.F., ROBERTSON, I.L., CORDEY, J.G. and FIELD, J.J. in Plasma Physics and Controlled Nuclear Fusion Research (Proc. of 8th Int.Conf. Brussels,1980) Paper IAEA-CN 38/W3.

[13] EUBANK, H., GOLDSTON, R., ARUNASALAM, V., BITTER,M, BOL,K., et al. Neutral Beam Heating Results, Princeton Plasma Physics Lab. Report PPPL-1491 (1978).

[14] COPPI, B. and MAZZUCATO, E., Phys.Lett.71A, No.4, (1979) 337.

[15] SPITZER, L., GROVE, D.J., JOHNSON, W.E. and WESTENDORP, W.F. NYO 6047 (1954).

[16] RIBE, F.L. Rev.Mod.Phys.47, (1975) 7.

[17] CARRUTHERS, R., in Controlled Fusion and Plasma Physics (Proc. 7th Eur.Conf. Prague, 1977) 2 (1977) 217.

[18] PFIRSCH, D., The Present State of Tokamak Research with Reference to Reactor Requirements (Proc.10th Symp.Fusion Technology, Padova 1978) 1, (Pergamon Press,1979) 433.

[19] STACEY, W.M., Nucl.Fusion 13, (1973) 843.

[20] OHTA,M., AMATO, H. and MORI, S. in Plasma Physics and Controlled Nuclear Fusion Research (Proc.4th Int.Conf.Madison 1971) 3, IAEA, Vienna (1971) 423.

[21] HOULBERG,W.A. and CONN, R.W., Nucl.Fusion 19,(1979) 81.

[22] BORRAS, K., LACKNER, K. and MINARDI, E., in Controlled Fusion and Plasma Physics (Proc.9th Eur.Conf.Oxford 1979) 1, (1979) 110.

[23] MILLS, R.G., A Fusion Power Plant, MATT-1050(1974).

[24] PETRIE, T.W. and RAWLS, J.M., Burn Control from Toroidal Field Ripple, General Atomic Co., Report GA-A15218(1979).

[25] ASHBY, D.E.T.F. and HUGHES, M.H., Nucl.Fusion, 20, (1980) 451.

[26] HIRSHMAN, S.P.Phys.Fluids, 19, 1, (1976) 155.

[27] DUCHS, D.F., POST, D.E. and RUTHERFORD,P.H.Nucl.Fusion 17, (1977) 565.

[28] TFR GROUP. Numerical Simulation of the Impurity Peak Positions in TFR 400 Discharges. Report No.EUR-CEA-FC-947.(1978).

[29] HAWRYLUK, R.J., SUCKEWER, S.and HIRSHMAN, S.P., Nucl.Fusion 19, (1979) 607.

[30] RUTHERFORD,P.H., Phys.Fluids, 17, (1974) 1782.

[31] SAMAIN, A and WERKOFF, F., Nucl.Fusion, 17, (1977) 53.

[32] Details of HERMES are available on request.

[33] McCRACKEN, G.M. and STOTT, P.E., Nucl.Fusion, 19, (1979) 889.

[34] HUGHES,M.H. and POST,D.E. Jour.Comp.Phys.28, No.1,(1978) 43.

[35] SYKES, A., and WESSON,J.A. Phys.Rev.Lett.44, No.18 (1980) 1215.

[36] APGAR, E., COPPI, B., GONDHALEKAR, A., HELAVA, H., KOMM, D., MARTIN,F., MONTGOMERY,B., PAPPAS, R., PARKER, R. and OVERSKEI,D. in Plasma Physics and Controlled Nuclear Fusion Research (Proc.6th Int.Conf.Berchtesgaden 1976) Vol.I.(1977) 247.

[37] AXON,K.B., CLARK, W.H.M., CORDEY,J.G., COX,M., FIELDING,S.J., GILL,R.D., HUGILL,J., LOMAS,P., PAUL, J.W.M., POWELL, B.A., PRENTICE,R., START, D.F.H. SUMMERS,D.D.R. and THOMAS,P. in Plasma Physics and Controlled Nuclear Fusion Research(Proc.8th Int.Conf. Brussels,1980) IAEA-CN-38/N4.

[38] KITSUNEZAKI,A., FUJISAWA,N., IOKI,K., KONOSHIMA,S., NAGAMI,M., OHARA,Y., OZAKI, N., SEKI,S., SHIMADA,M., SUGAWARA,T., TOYAMA,H., YOKOMIZO,H, in Plasma Physics and Controlled Nuclear Fusion Research (Proc.8th Int.Conf.Brussels,1980) IAEA-CN-38/N-3.

[39] SPITZER, L., HARM, R., Phys.Rev.89, (1953) 977.

[40] HINTON, F.L. and HAZELTINE, R.D. Rev.Mod.Phys.48,(1976) 239.

[41] PFEIFFER, W. and WALTZ, R.E. Nucl.Fusion,19, (1979) 51.

[42] AXON, K.B., BAXTER, G.A., BURT, J., CLARK, W.H.M., McCRACKEN, G.M., FIELDING, S.J., GILL, R.D., GOODALL, D.H.J., HOBBY, M., HUGILL, J., PAUL,J.W.M., POWELL, B.A., PRENTICE, R., REID, G.W., STOTT, P.E., SUMMERS, D.D.R. and WOOTTON, A.J. in Plasma Physics and Controlled Nuclear Fusion Research (Proc.7th Int. Conf.Innsbruck, 1978) Vol.I, IAEA. Vienna(1979) 51.

[43] ENGELHARDT, W., KLUBER,O., MEISEL,D., MURMAN,H., SESNIC,S., FUSSMANN,G., GLOCK,E., GOTTARDI,N., KARGER,F.,LISITANO,G., MAYER,H.M. and WAGNER,F.in Plasma Physics and Controlled Fusion Research (Proc.7th Int.Conf.Innsbruck, 1978) Vol.I, IAEA,Vienna (1979) 123.

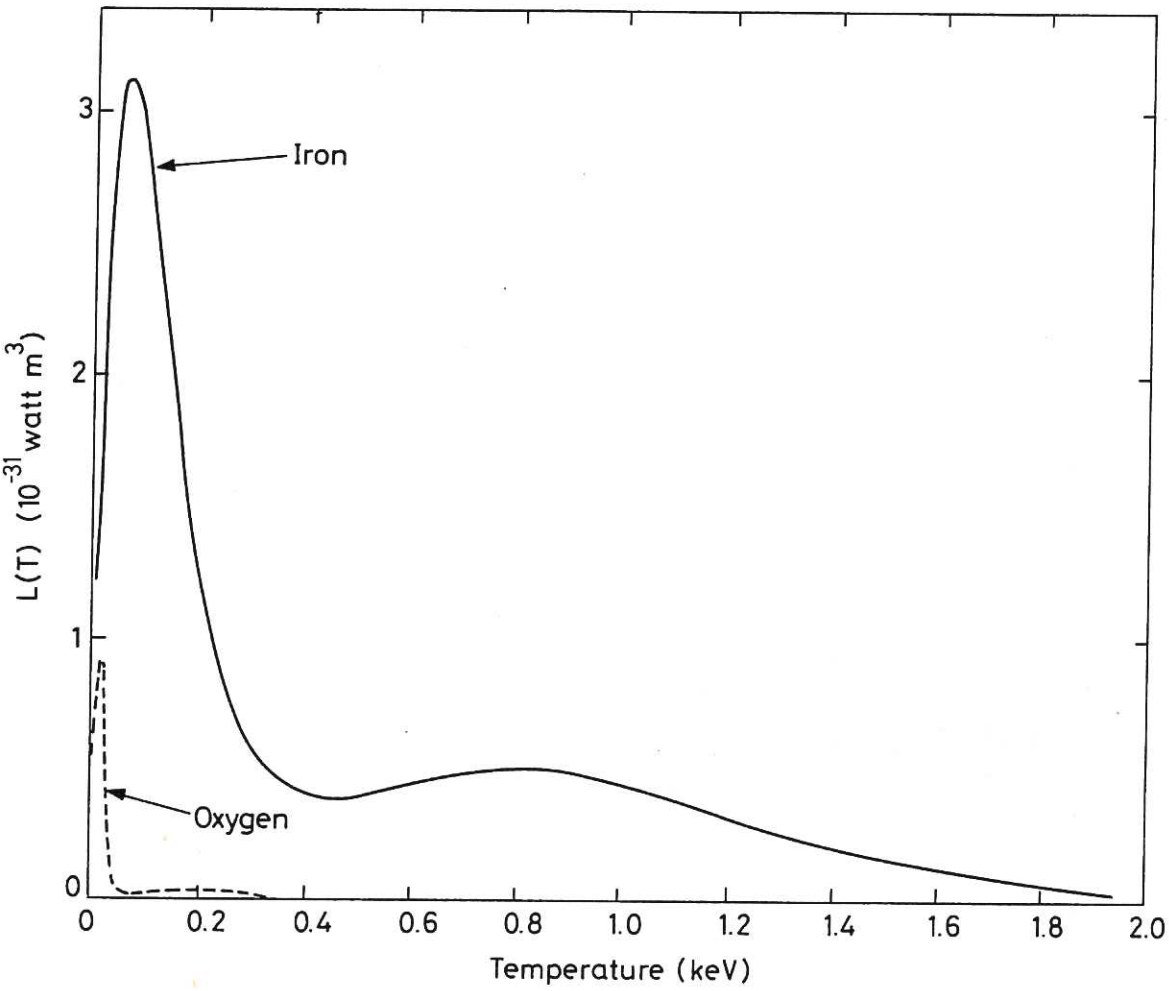

Fig.1 Radiation cooling rates for iron and oxygen taken from results by Post et al [9].

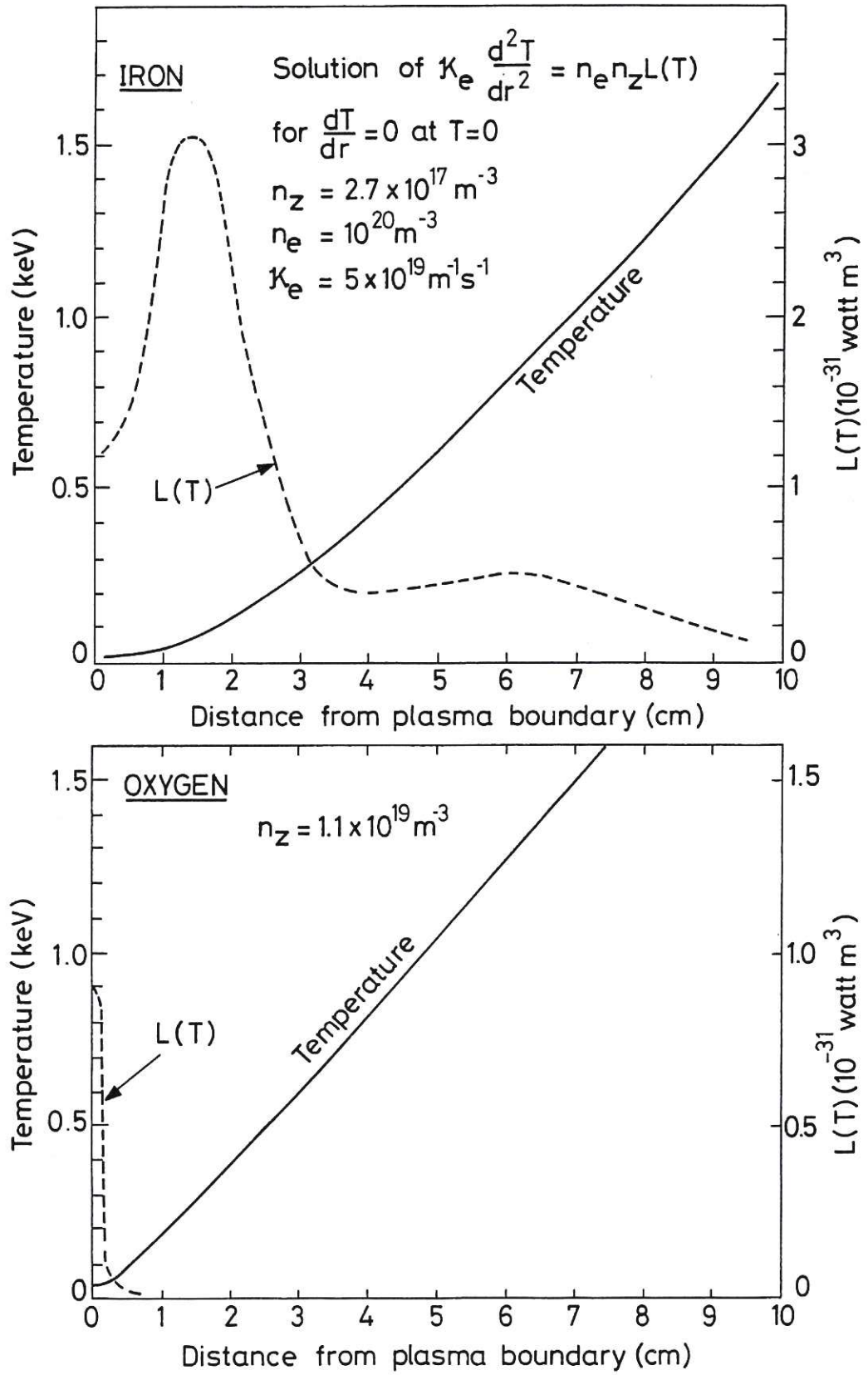

Fig.2 Temperature profiles and L(T) in INTOR when all the input power (50 MW) is radiated from the peripheral plasma by either iron or oxygen impurity, $n_e = 10^{20}\ m^{-3}$, n(iron) = $2{\cdot}7 \times 10^{17}\ m^{-3}$, n(oxygen) = $1{\cdot}1 \times 10^{19}\ m^{-3}$.

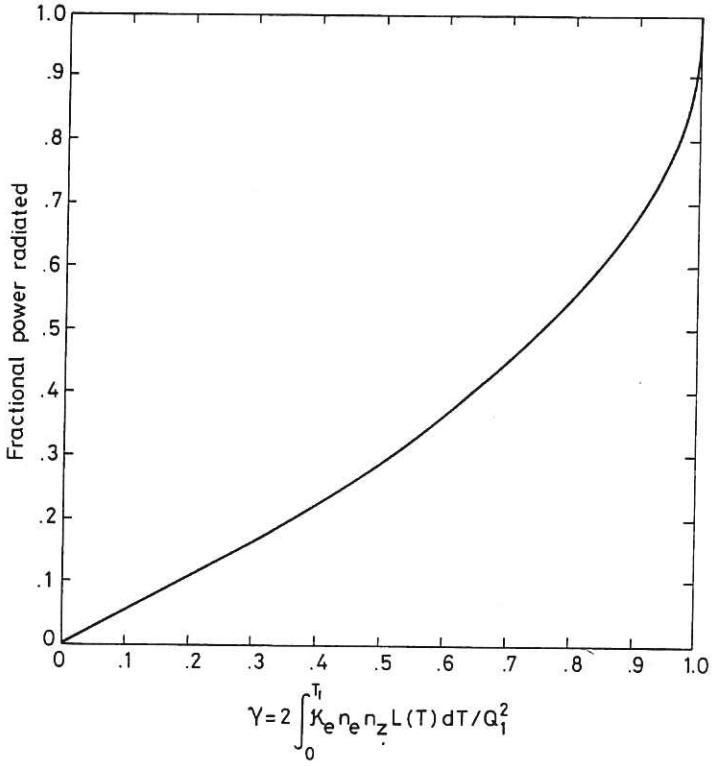

Fig.3 Fractional power radiated from the peripheral plasma as a function of $\gamma = 2\int_0^{T_1} \kappa_e n_e n_z L(T_e) dT_e/Q_1^2$ where Q_1 is the thermal flux transported into the peripheral plasma.

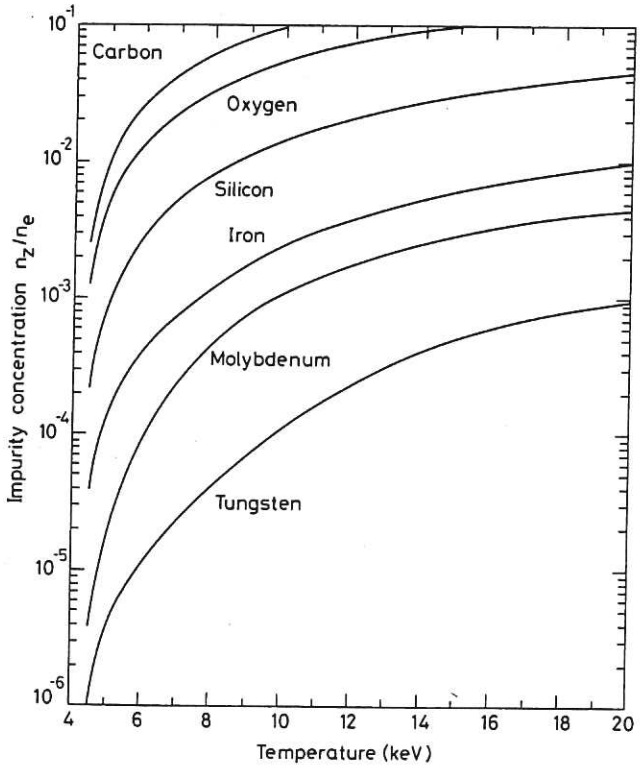

Fig.4 Maximum allowed impurity concentration in the central plasma as given by Jensen et al [4].

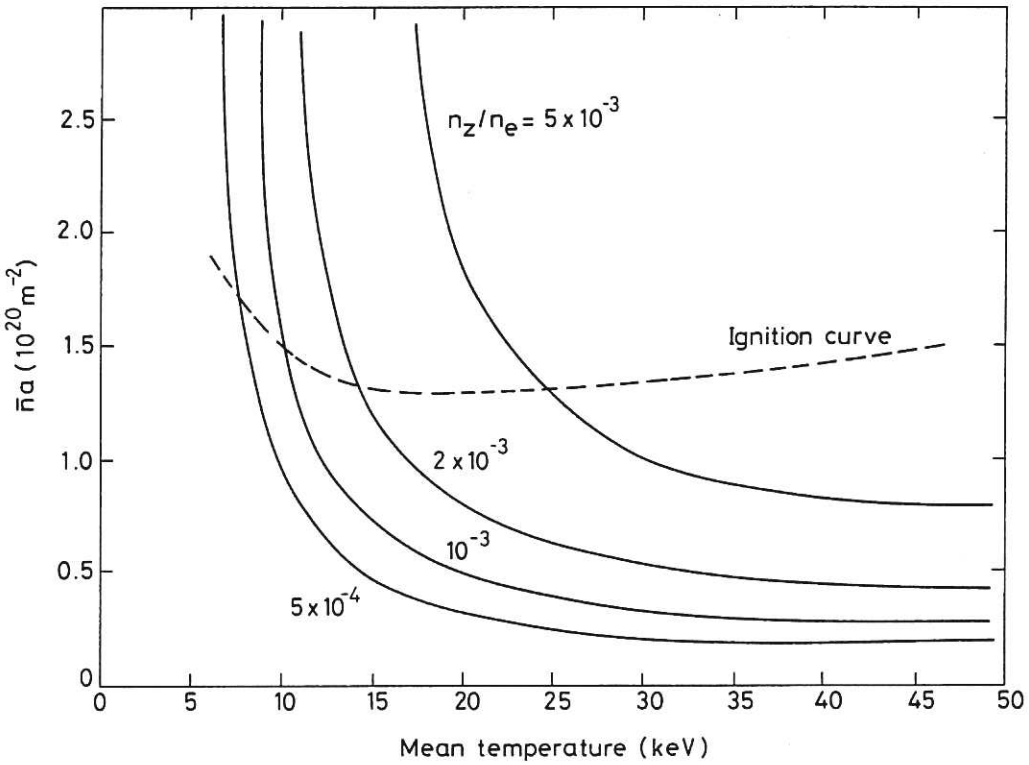

Fig.5 Contours of n_z/n_e at which the fusion power is balanced by peripheral radiation from iron impurity for $\kappa_e = 5 \times 10^{19}\ m^{-1}\ s^{-1}$.

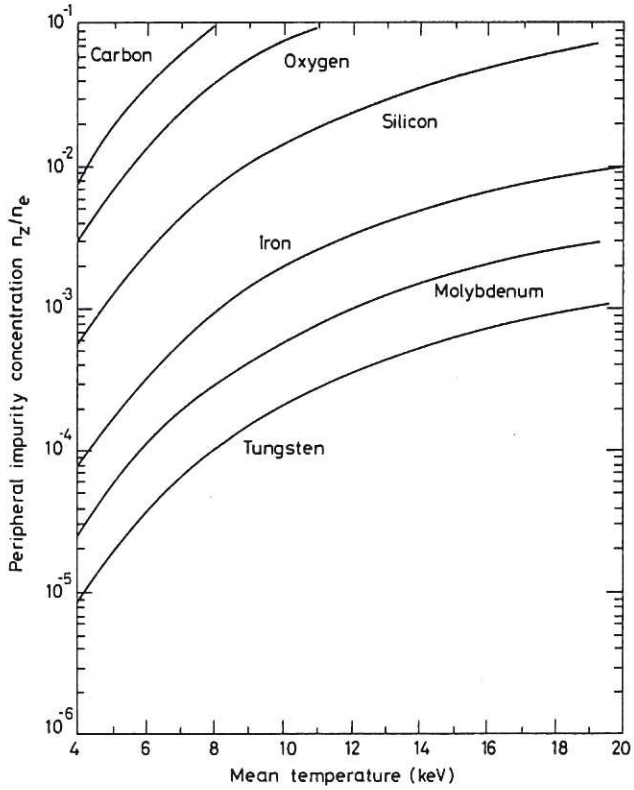

Fig.6 Maximum allowed impurity concentration in the peripheral plasma. This figure should be compared with Fig.4.

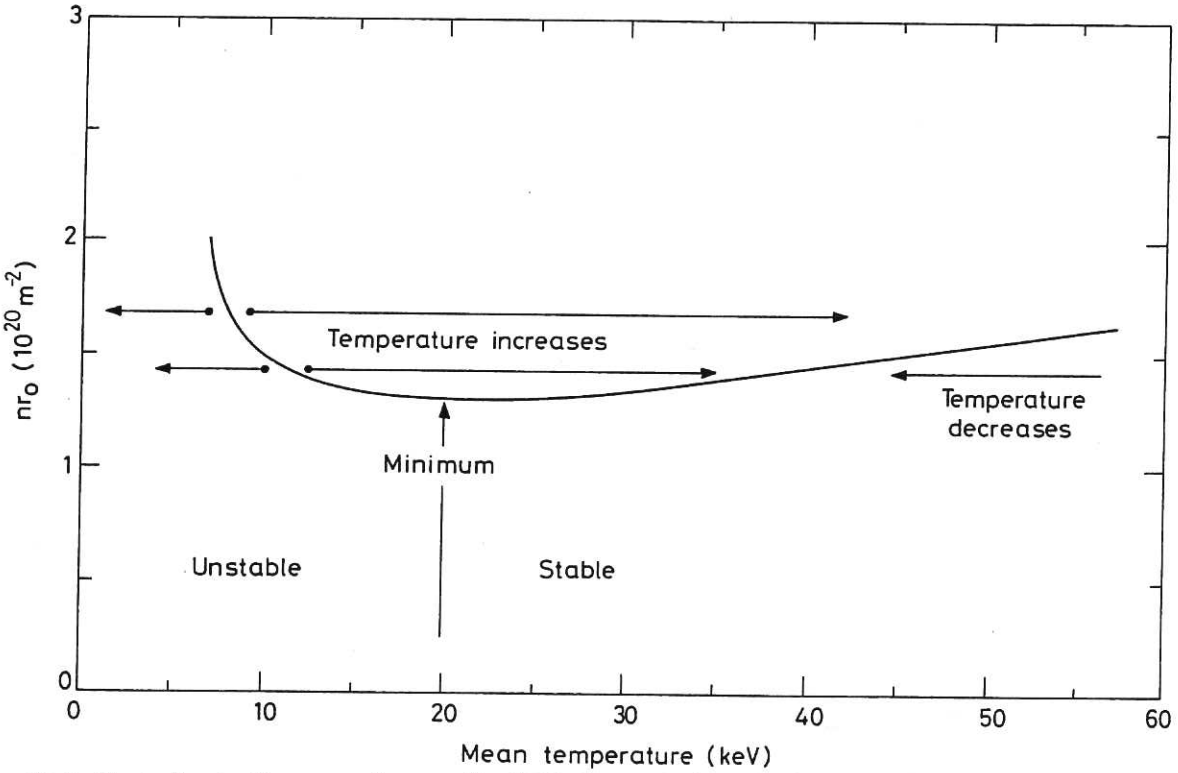

Fig.7 Illustrative ignition curve for a confined DT plasma. Trajectories for points just off the curve are shown. To the left of the minimum the curve is thermally unstable; to the right it is stable.

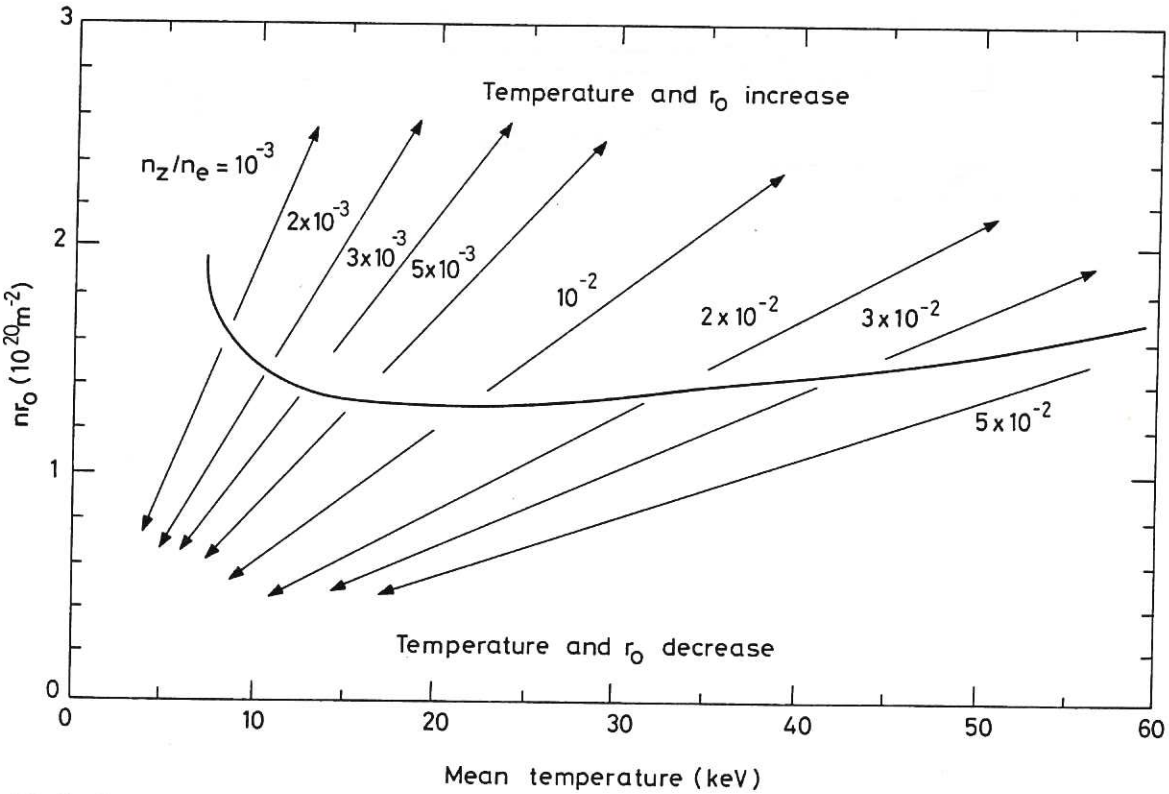

Fig.8 Illustrative ignition curve for a confined DT plasma. The trajectories for points just off the curve correspond to the case when all the alpha particle power is radiated by iron in the peripheral plasma and the T = 0 point is free to move. The entire ignition curve is thermally unstable.

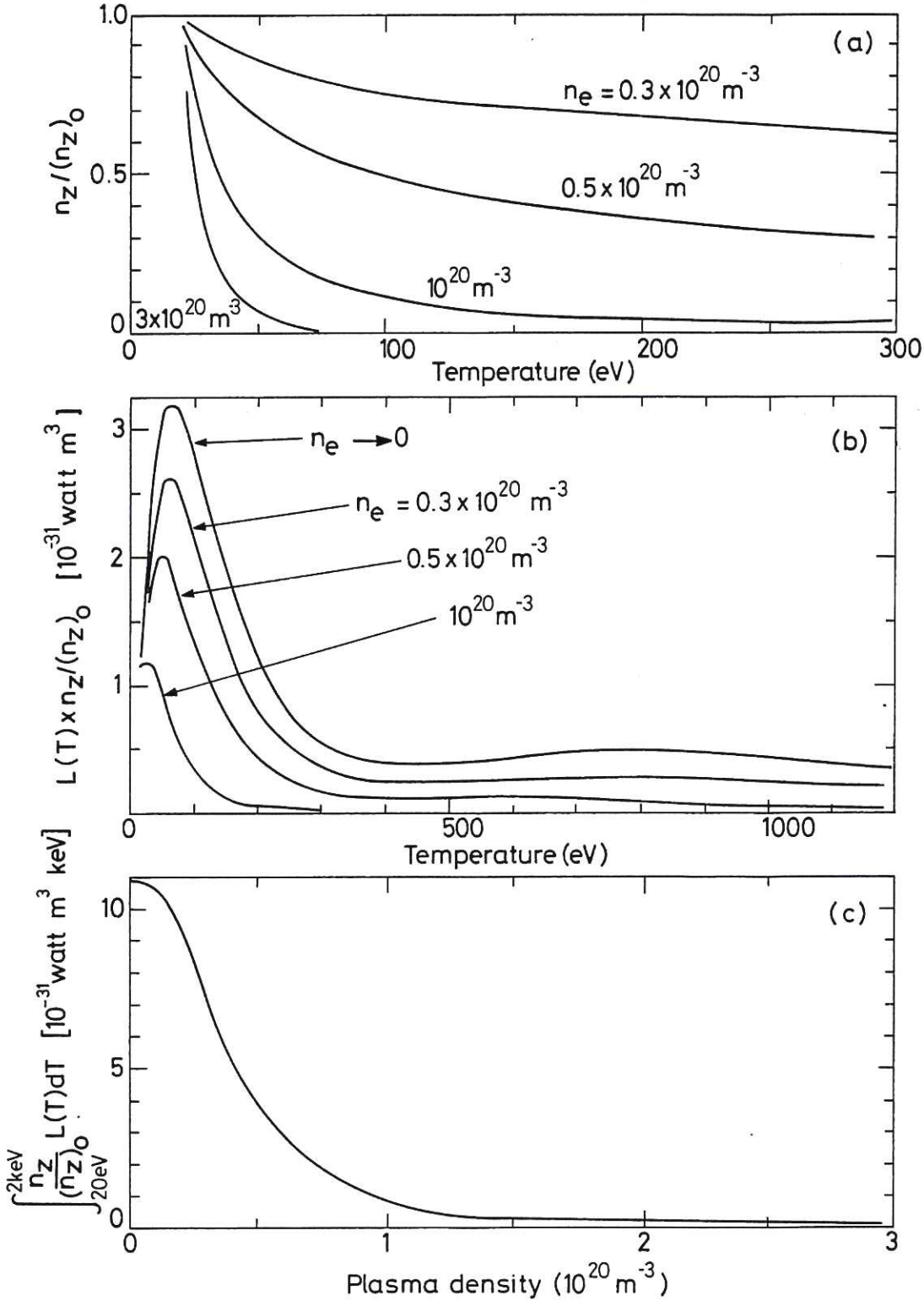

Fig.9 (a) n_z as a function of T at equilibrium for iron. Derived from $\Gamma_z = -D_{AN} \frac{dn_z}{dr} + D_o \left\{ \langle Z \rangle \frac{n_z}{n_H} \frac{dn_H}{dr} - \frac{dn_z}{dr} - \left(\frac{\langle Z \rangle}{2} + 1 \right) \frac{n_z}{T} \frac{dT}{dr} \right\} = 0$ and $\frac{1}{n_H} \frac{dn_H}{dr} \ll \frac{1}{n_z} \frac{dn_z}{dr}$ and $\frac{1}{T} \frac{dT}{dr}$.

(b) $n_z L(T)$ as a function of T for different values of n_e. (c) $\int_{20eV}^{2keV} n_z L(T)\, dt$ as a function of n_e.

Note: The expression for Γ_z assumes that 'temperature screening' is always present: this assumption is invalid as $T \rightarrow 0$ and the hydrogen ions become collissional.

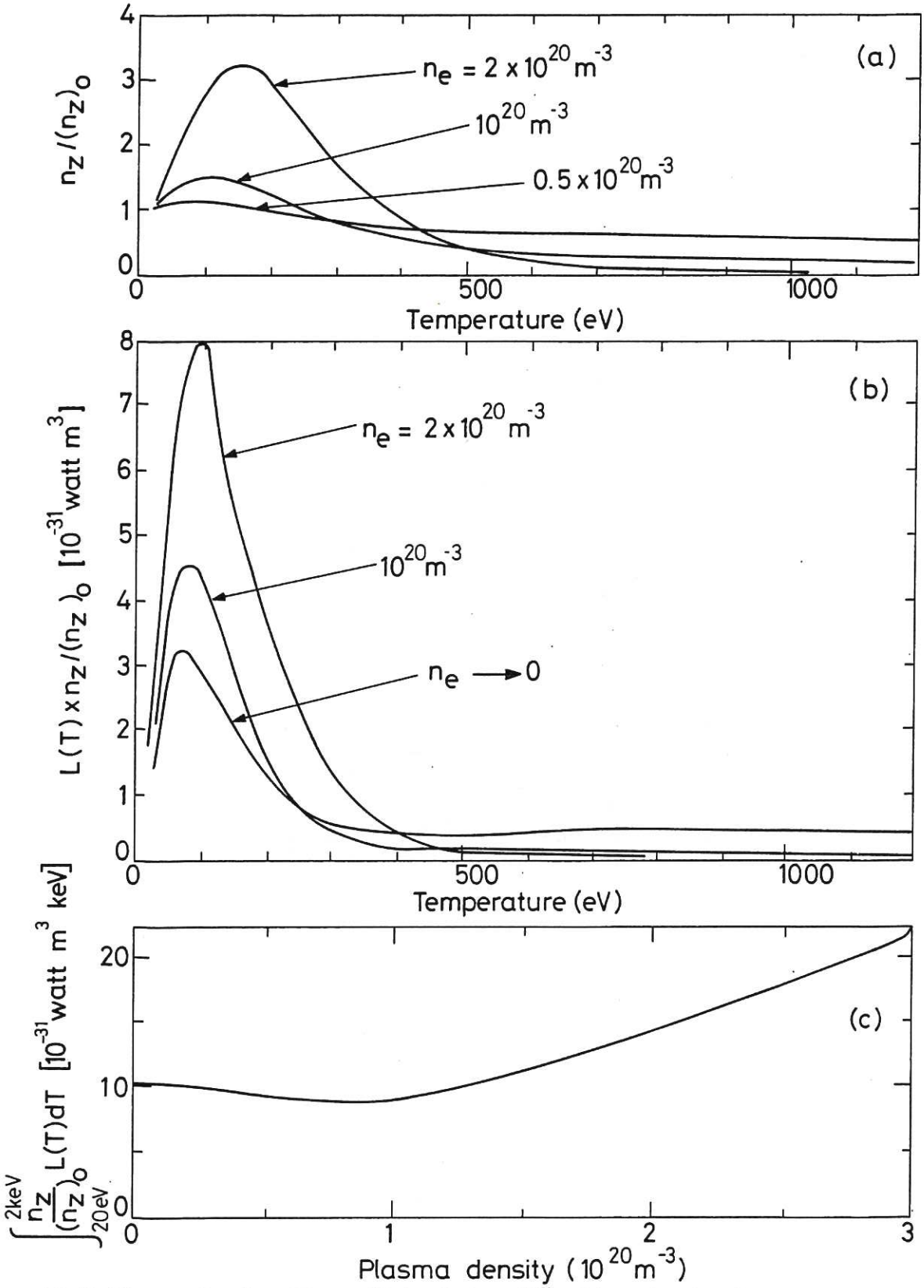

Fig.10 (a) n_z as a function of T at equilibrium for iron. (b) $n_z L(T)$ as a function of T.
(c) $\int_{20\,eV}^{2\,keV} n_z L(T)dT$ as a function of n.

Note: In these results 'temperature screening' is not present when the hydrogen ions are collisional. These figures should be compared with those in Fig.9 where 'temperature screening' is retained as $T \rightarrow 0$.

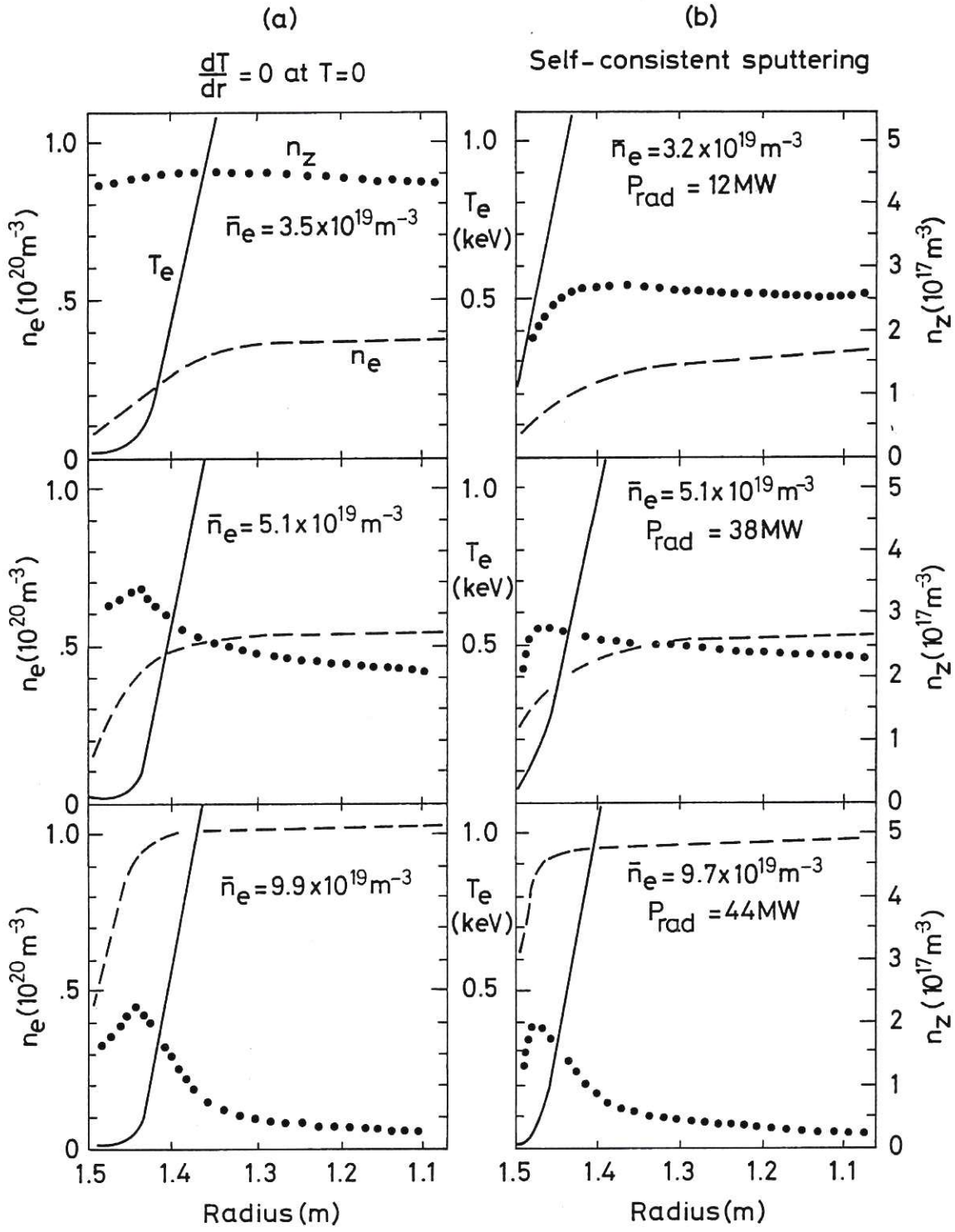

Fig.11 (a) Profiles of n_e, n_z and T_e when the plasma radiates all the input power so that $dT/dr = 0$ at $T = 0$. The examples correspond to INTOR at three different densities with 50 MW of input power. The impurity is iron. (b) Similar profiles when n_z is determined by self-consistent sputtering by neutrals. As $\bar{n}_e$ is increased the influx of sputtered iron atoms drops as follows: $7{\cdot}2 \times 10^{18}$ m^{-2} s^{-1} : $4{\cdot}2 \times 10^{18}$ m^{-2} s^{-1} : $9{\cdot}7 \times 10^{17}$ m^{-2} s^{-1}.

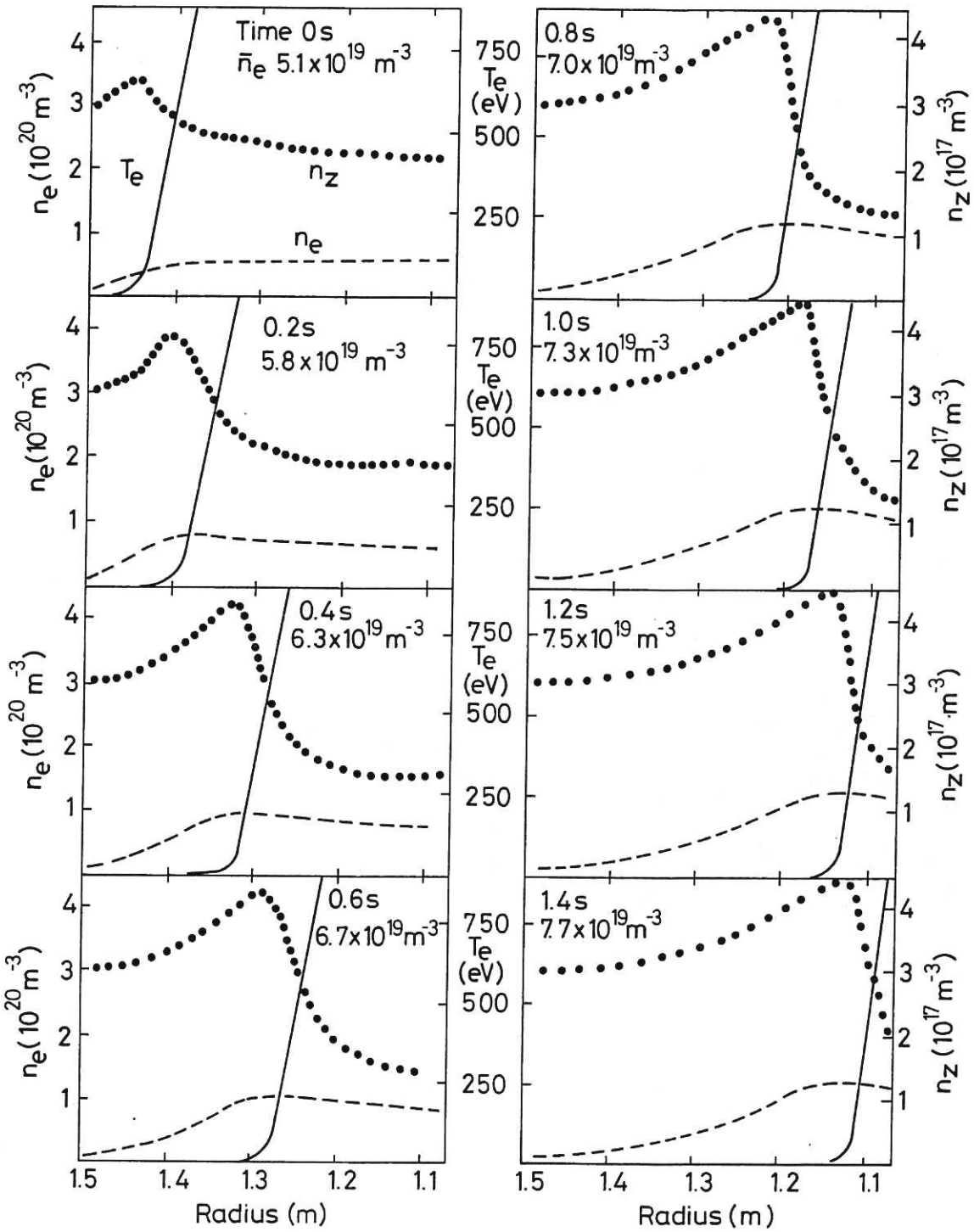

Fig.12 Profiles of n_e, n_z and T_e when temperature profile collapse is caused by increasing the recycling coefficient from unity to 1·1 at t = 0 s thus causing the density to increase. Initial energy confinement time = 0·8 s.

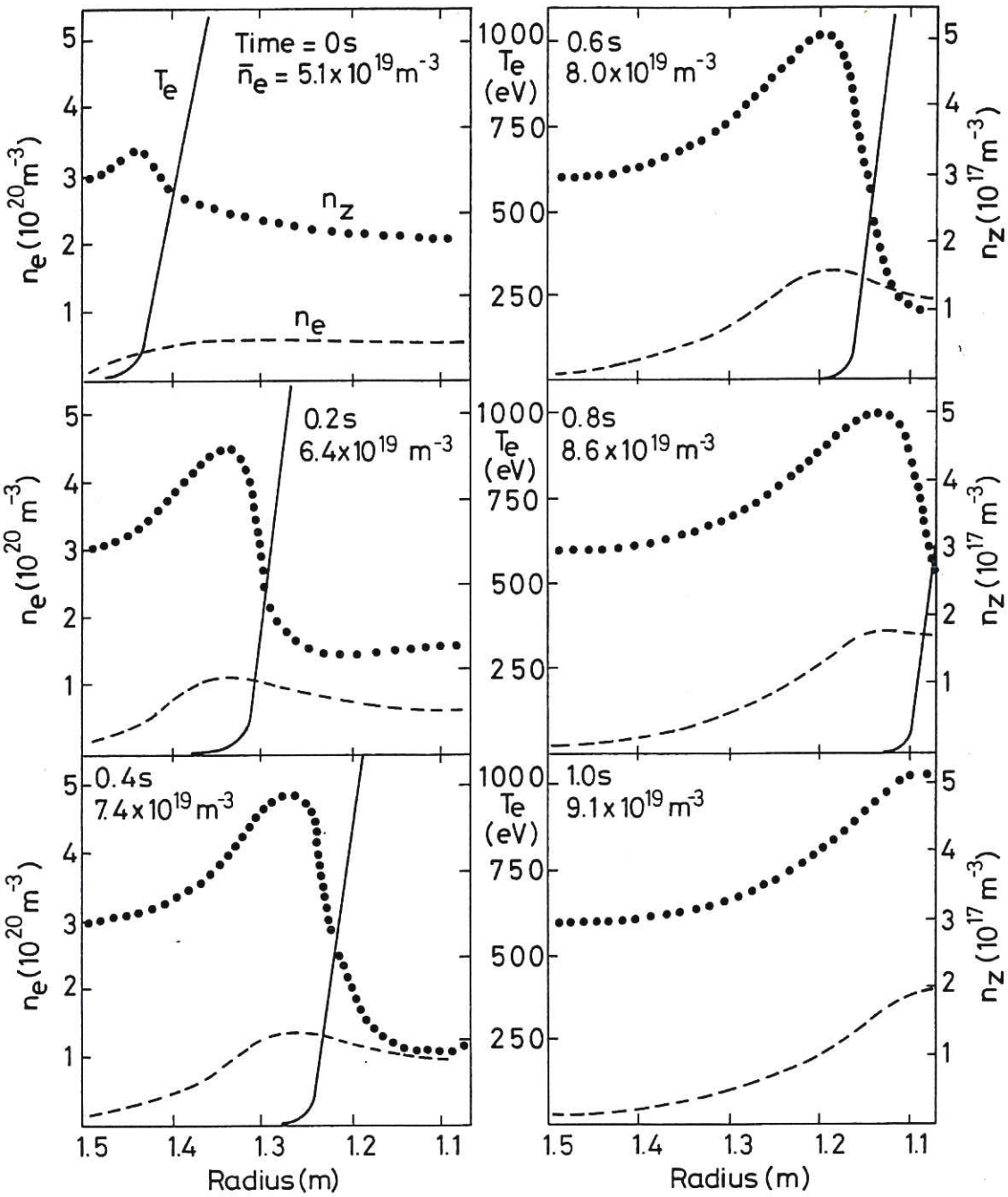

Fig.13 Profiles of n_e, n_z and T_e when the recycling coefficient is increased from unity to 1·2. The temperature collapse is faster than the case shown in Fig.12.

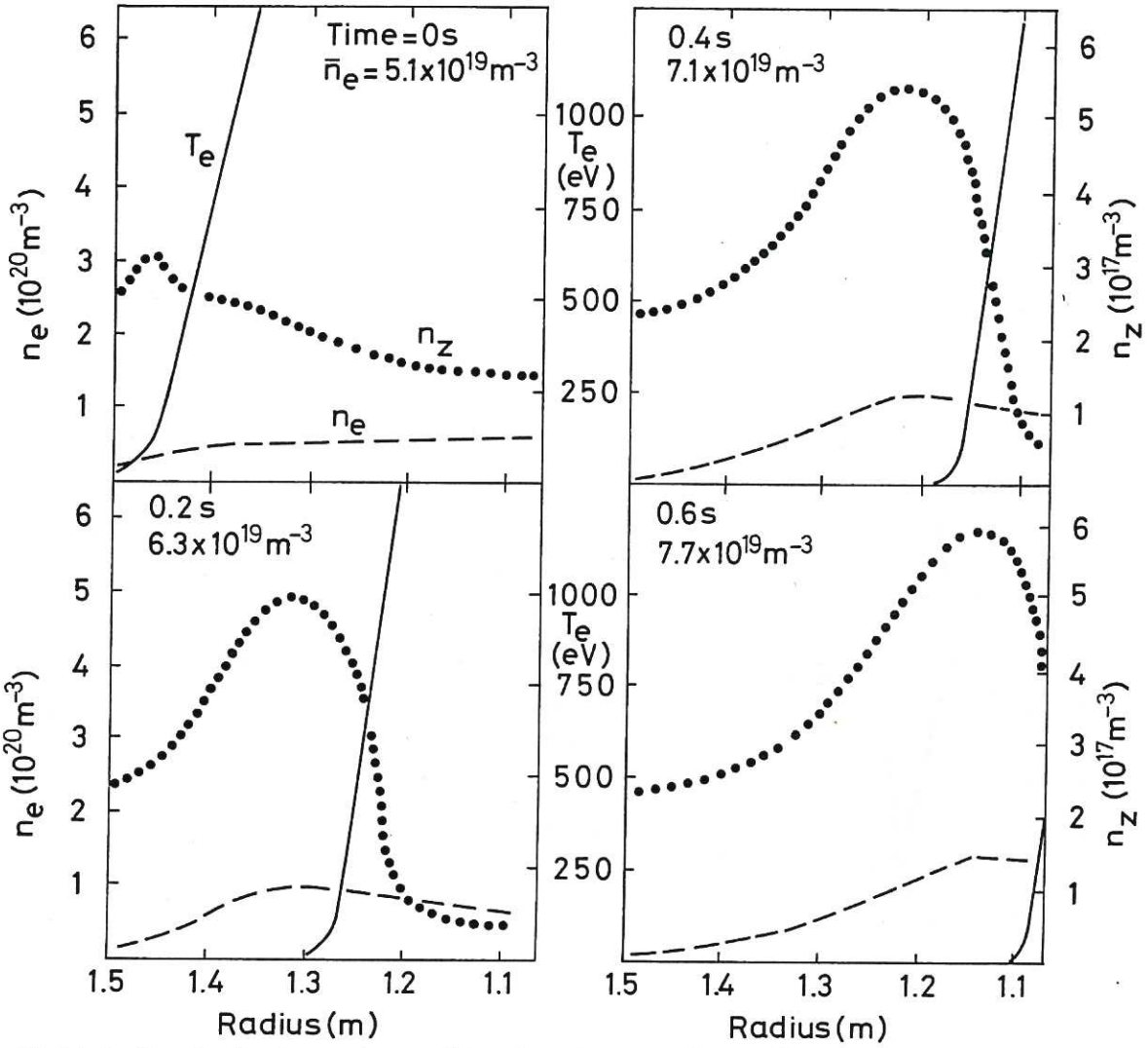

Fig.14 Profiles showing temperature profile collapse for a recycling co-efficient of 1·2. In this case I = 2 MA instead of 4 MA, as was the case for Fig.13. The reduction in I increases q and hence enhances neoclassical effects.

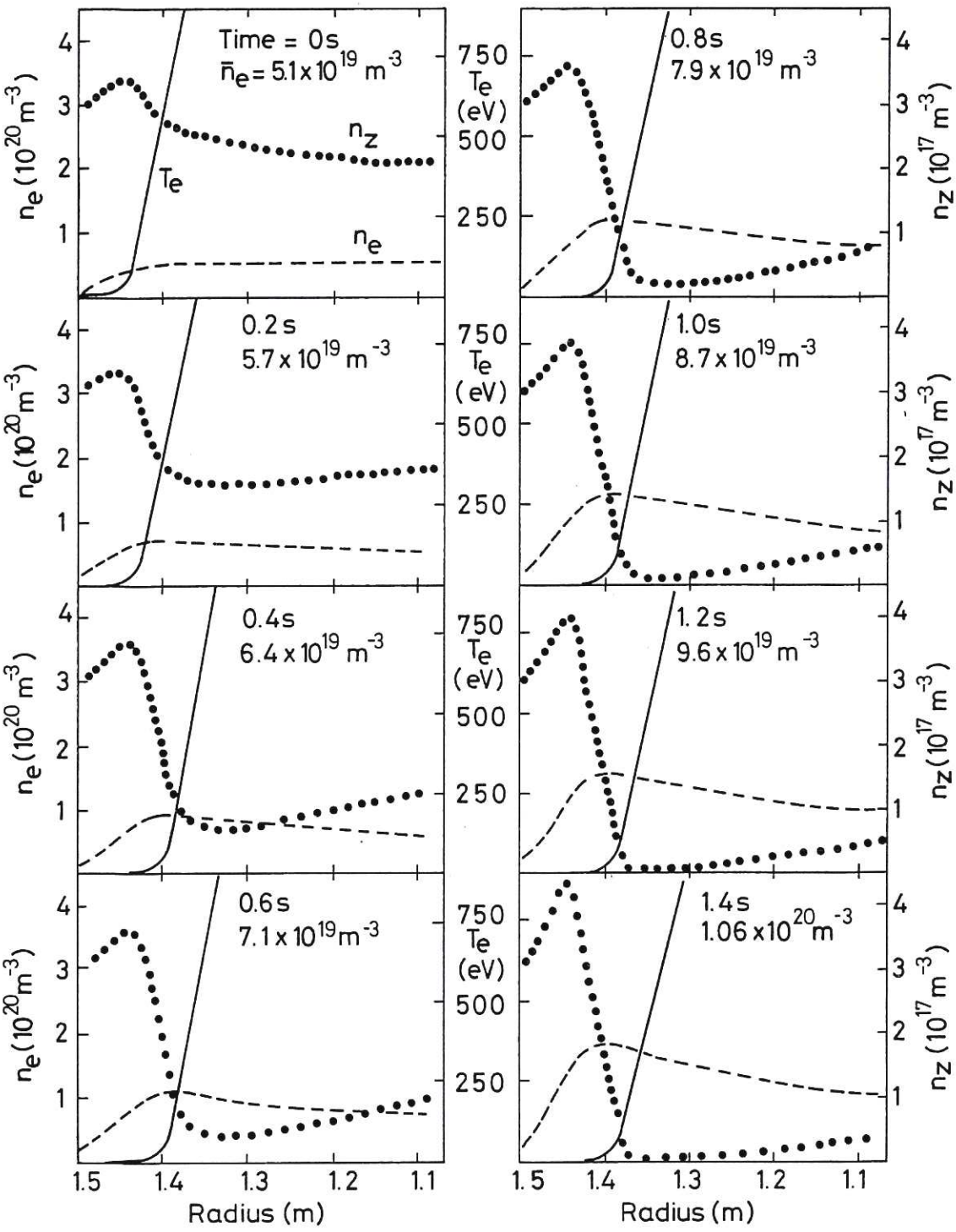

Fig.15 Profiles showing the effect of retaining 'temperature screening' as $T \to 0$ and the hydrogen ions become collisional. This figure should be compared with Fig.12. The conditions are identical except that for the case illustrated above eqn.18 was used to describe the impurity transport at all temperatures.

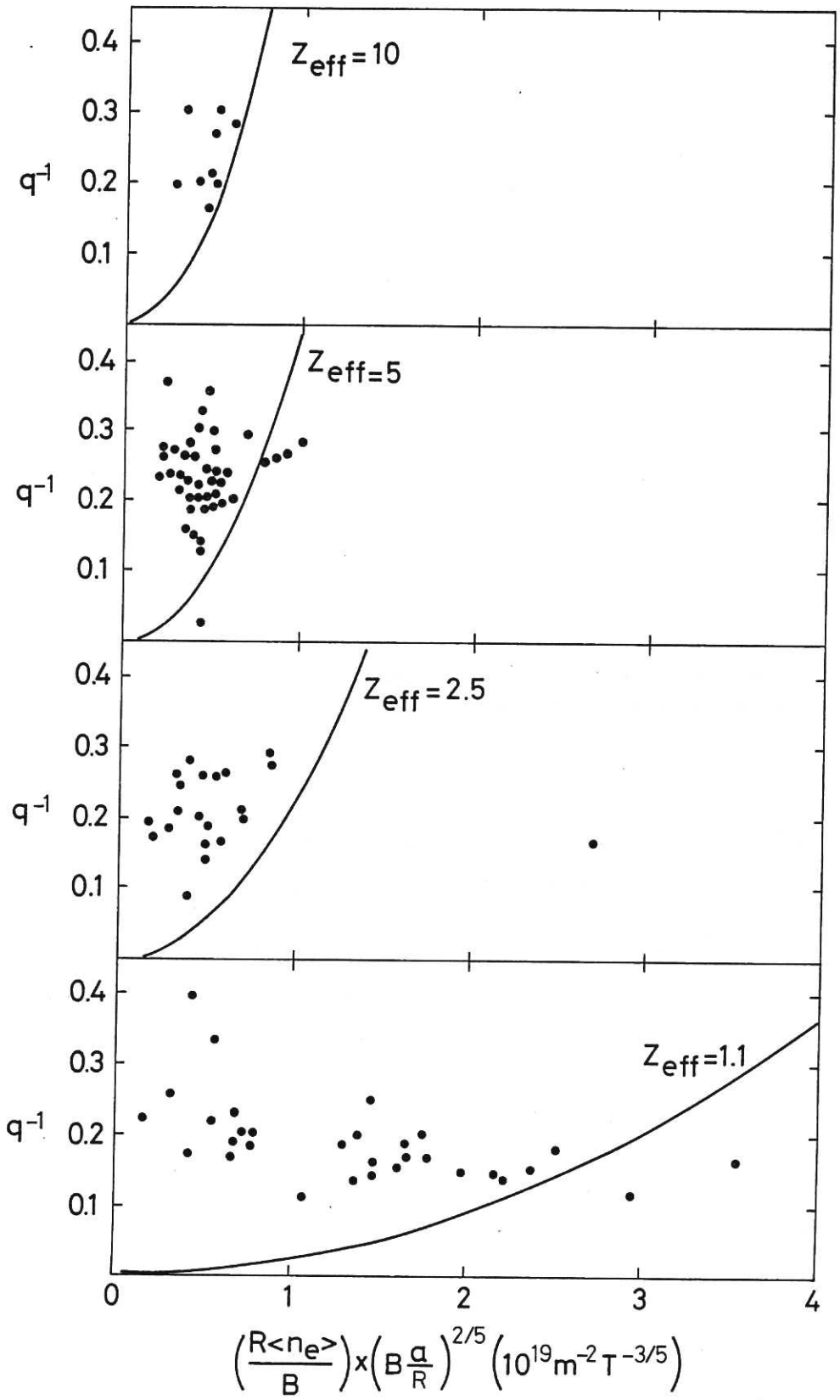

Fig.16 The density limit for ohmic-heated tokamaks given by eqn.37 for four values of Z_{eff}. The points are from the experimental data compiled by Pfeiffer and Waltz [41]. The top figure shows discharges with $Z_{eff} \geqslant 10$; The remainder refer to discharges with $10 > Z_{eff} \geqslant 5$, $5 > Z_{eff} \geqslant 2{\cdot}5$ and $2{\cdot}5 > Z_{eff} \geqslant 1$ respectively.

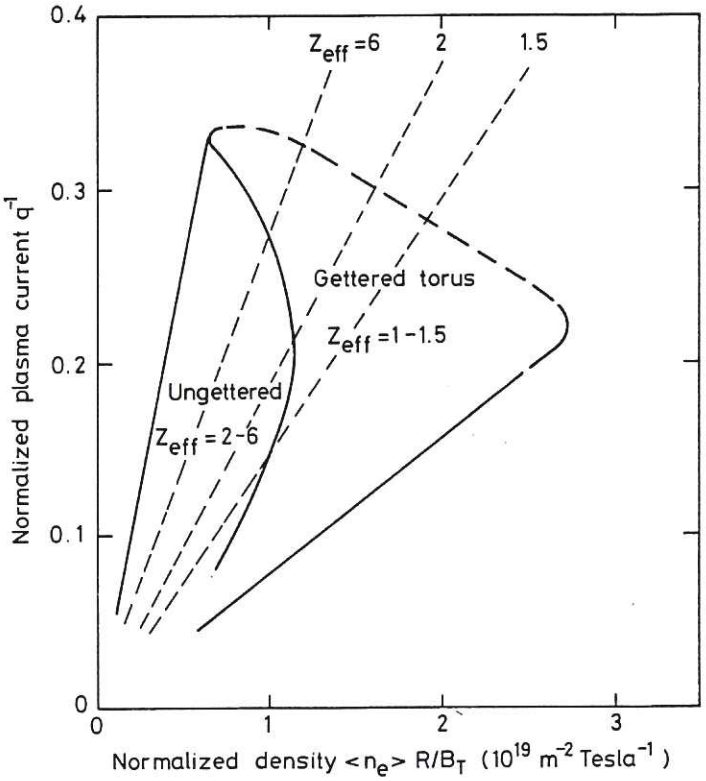

Fig.17 Density limits for the DITE tokamak for ohmic-heated discharges [37]. For comparison the limit set by eqn.(34) is also shown for Z_{eff} = 1·5, 2 and 6 on the assumption that $\bar{T}$ = 300 eV.

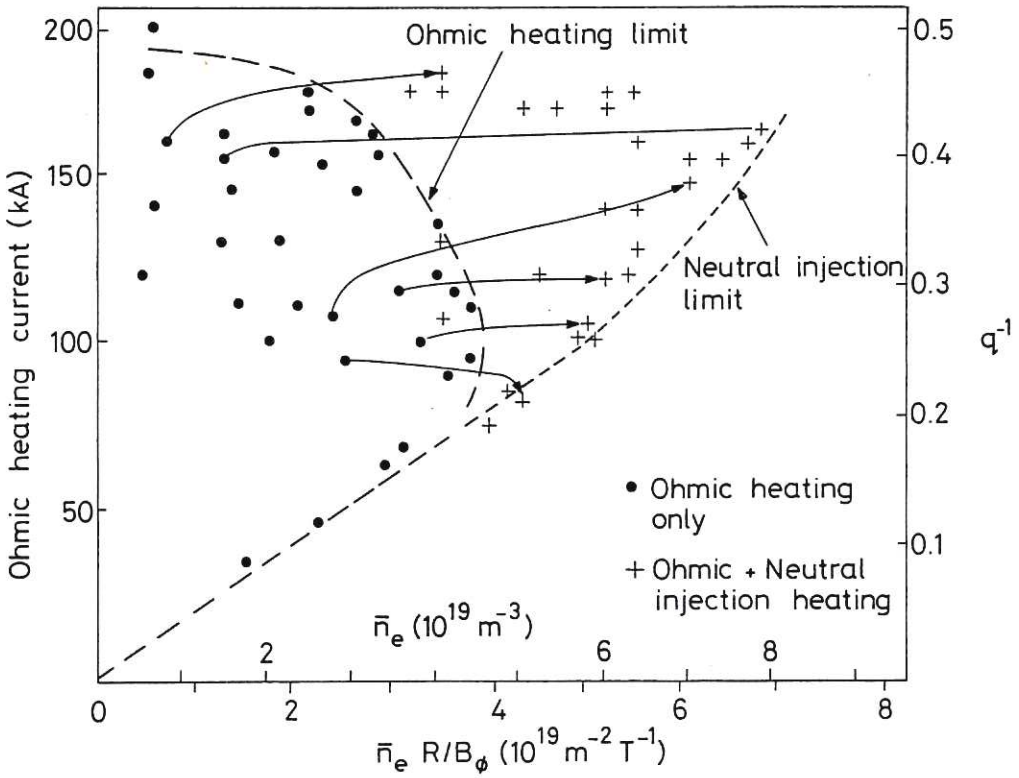

Fig.18 Density limits for the DITE tokamak for ohmic-heating alone and additional neutral beam heating. The magnetic field is constant at 1·35 Tesla.

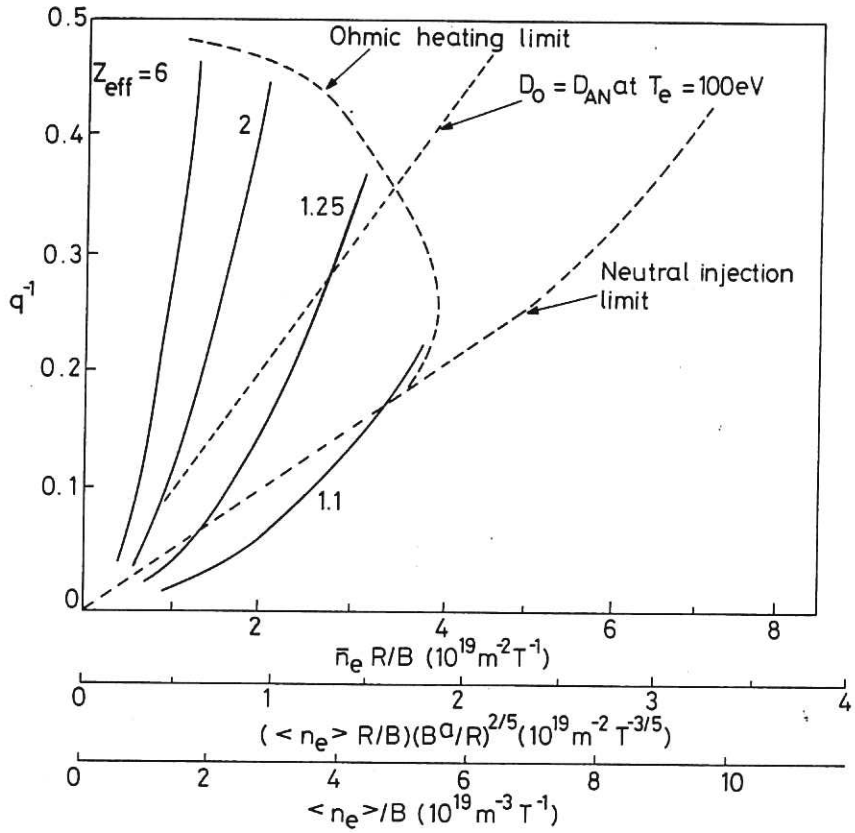

Fig.19 Density limit for the DITE tokamak shown in Fig.18 compared with eqn.(37). Also shown is the line $D_{AN} = D_O$ where neoclassical effects become noticeable. Note $\bar{n}_e$ refers to line average and $\langle n_e \rangle$ volume average; the latter is used in eqns.(37) and (40).

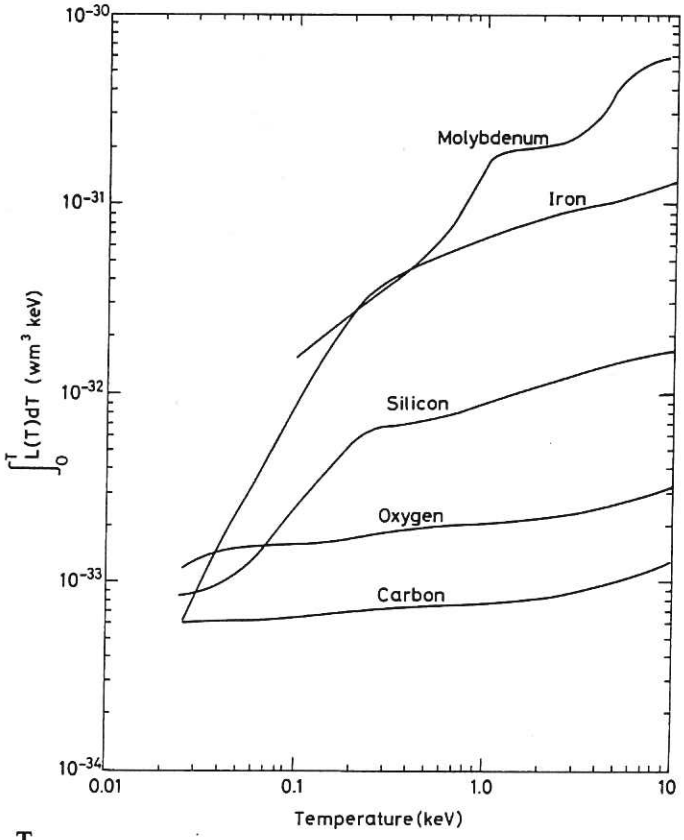

Fig.A1 $\int_0^T L(T)dT$ as a function of temperature for some common impurities.

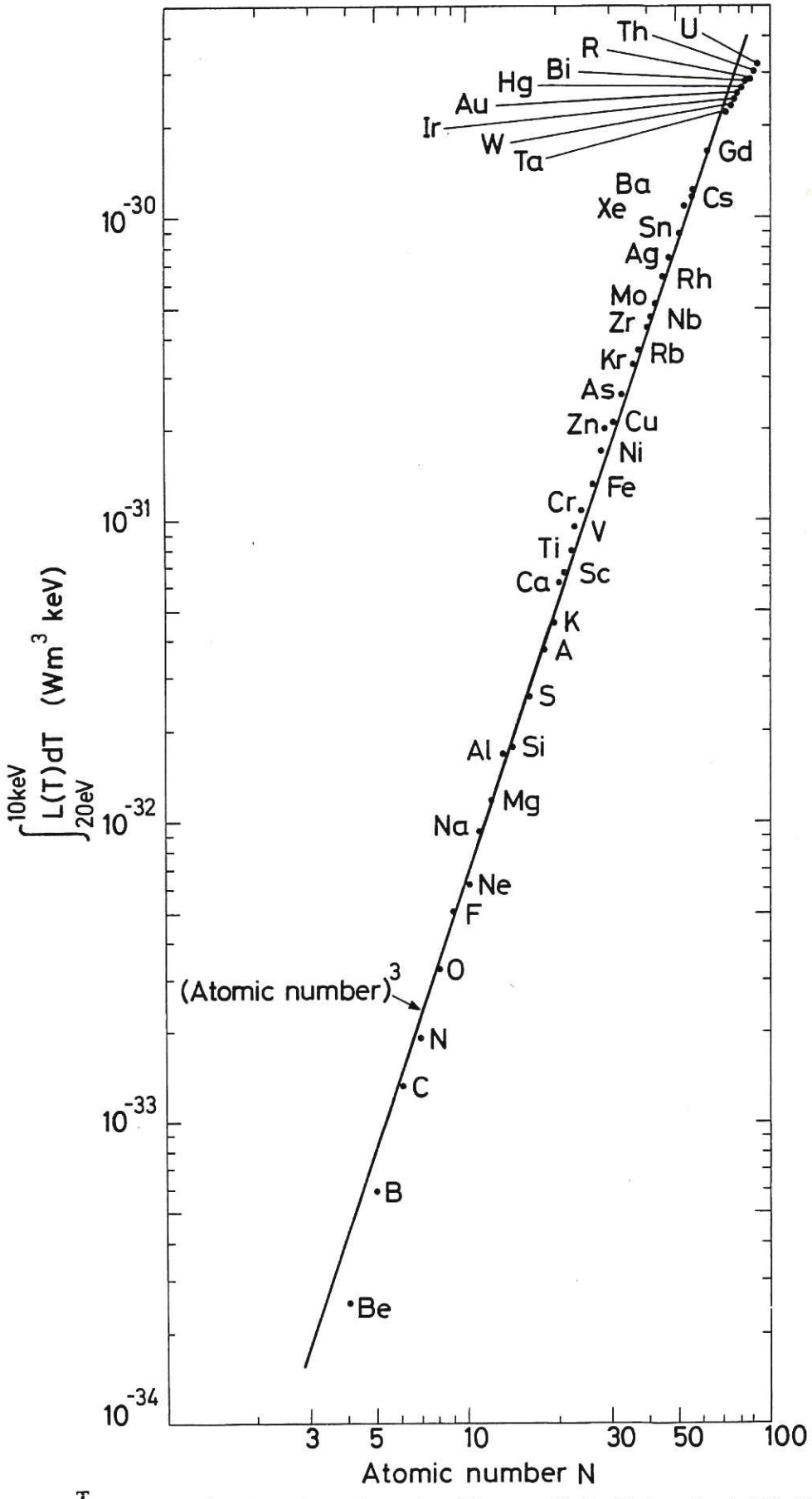

Fig.A2 $\int_0^T L(T)dT$ as a function of atomic number. The upper limit of integration is 10 keV.

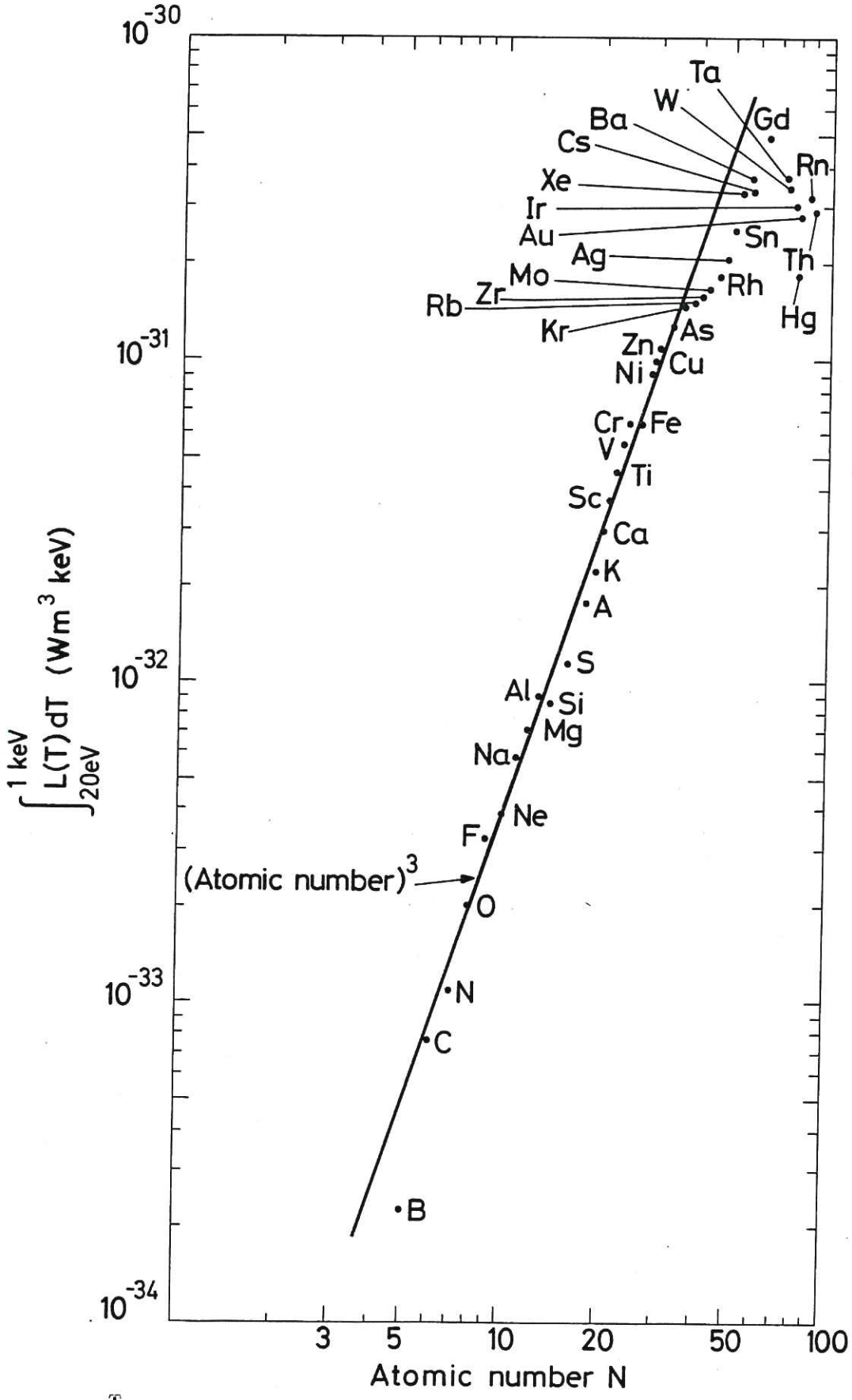

Fig.A3 $\int_0^T L(T)dT$ as a function of atomic number. The upper limit of integration is 1 keV. This figure should be compared with Fig.A2 where the integration limit was 10 keV.